SURFACE ENERGY BUDGET OVER INLAND WATER

By

QIANYU ZHANG

A thesis submitted in partial fulfillment of
the requirements for the degree of

MASTER OF SCIENCE IN ENVIRONMENTAL ENGINEERING

WASHINGTON STATE UNIVERSITY
Department of Civil and Environmental Engineering

MAY 2012

To the Faculty of Washington State University:

The members of the Committee appointed to examine the thesis
of Qianyu Zhang find it satisfactory and recommend that it be accepted.

_____

Heping Liu, Ph.D., Chair

_____

Brian Lamb, Ph.D.

_____

Shelley Pressley, Ph.D.

_____

Jennifer Adam, Ph.D.

Acknowledgements

I am grateful to Dan Gaillet, Billy Lester, Jennifer Taylor, Jason Temple, and many other people in Pearl River Valley Water Supply District in Ridgeland, Mississippi, as well as Yu Zhang, Haimei Jiang, Li Sheng, Rongping Li, Yu Wang, and Guo Zhang who contributed to field work.

I would like to give special thanks to my advisor, Dr. Heping Liu, for all the science and writing training I received. I would have no chance to finish this thesis if not with his great patience, diligence, and inspiration. I found it was a great fortune to work with him.

I would like to thank the committee members, Dr. Brian Lamb, Dr. Shelley Pressley, and Dr. Jennifer Adam, for the advices and opportunities that have strengthened my research experience. Thanks to Dr. Tom Jobson, for his teaching in the useful software technique and advices for surviving in graduate school. I thank all faculty, staff and graduate students at LAR and the Department of Civil and Environmental Engineering for their great supports. I thank many friends who make my stay wonderful at Pullman.

Finally, I owe much gratitude to my husband. For his consistent support, I was able to persist and work hard on this thesis. I thank my Dad and Mom very much for their moral and financial support throughout my study at WSU.

SURFACE ENERGY BUDGET OVER INLAND WATER

Abstract

By Qianyu Zhang, M.S.
Washington State University
May 2012

Chair: Heping Liu

To better understand water-atmosphere interactions requires direct measurements of the surface energy budget and trace gas exchange over inland waters. In this study, an eddy covariance system was used to measure turbulent fluxes of sensible (H) and latent heat (LE) in 2008 and 2009 over the Ross Barnett Reservoir (hereafter “the Reservoir” which was ice-free) in Mississippi, U.S.A., to study physical processes that control daily, intra-seasonal, seasonal, and interannual variations in the surface energy budget.

Our results indicate that H and LE were distinctively out-of-phase with net radiation (Rn) on different timescales. Fueled by the previously stored heat in the water, the turbulent transfer of H and LE from the water to the atmospheric surface layer (ASL) was still substantial on nights with

a negative Rn and in winters when Rn was very small. The annual means of net radiation, H, and LE for the two years were 110.6, 15.7, and 83.7 W m^{-2}, respectively. About 81% of the Rn absorbed by the water was transferred to the atmosphere through LE and the remainder was transferred through H. On a monthly basis, the upward, positive temperature and humidity gradients, the unstable ASL, and the sufficient mechanical mixing were observed, leading to persistent positive H and LE. Intraseasonal and seasonal variations in turbulent exchanges of H and LE were strongly affected by alternative incursions of large-scale air masses brought in by different synoptic weather systems (e.g., cyclones or anticyclones) throughout the two years. Southerly winds with tropical maritime air masses (warm and humid) from the Gulf of Mexico and northerly winds with continental air masses (cool and dry) produced two distinctive atmospheric forcings for the water-air interactions. Interannual variability in the surface energy budget was modulated by variations in mean climate conditions as well as by differences in these synoptic weather events. It suggests that possible shifts in northerly and southerly winds associated with changes in synoptic weather events would have significant impacts on seasonal, annual, and interannual variations in the water surface energy budget, evaporation rates, and hydrologic processes in this region.

Table of Contents

List of Figures

List of Tables

Symbols

α	Albedo
ASL	Atmospheric surface layer
B	Bowen ratio, calculated as sensible heat flux divided by latent heat flux
C_E	Bulk transfer coefficients for moisture
C_H	Bulk transfer coefficients for heat
C_p	Specific heat of air
C_{pw}	Specific heat of water
Ctrn.Flux(PS)%	Contribution of the flux in percentage to the overall flux
cumE	Cumulative evaporation
Days(PS)	Pulse days with H and LE pulses
e_a	Atmospheric vapor pressure
e_w	Saturation vapor pressure at the water surface layer temperature, T_w
Δe	$\Delta e = e_w - e_a$, vertical gradient of vapor pressure over the water surface
EBC	Energy balance closure
EBEX	Energy balance experiment
Flux(PS)	Averaged daily mean of the flux during the pulse days
G	Heat flux into the water
GSL	Great Slave Lake
H	Sensible heat flux
IRGA	Open path CO_2/H_2O infrared gas analyzer
JFM	January, February, and March
JJA	June, July, and August
K_p	Penetrating solar radiation through water surface into deeper layers
K↓	Incident shortwave radiation
K↑	Reflected shortwave radiation
L	Latent heat of vaporization
L↓	Incoming longwave radiation
L↑	Outgoing longwave radiation
LE	Latent heat flux
LT	Local time

ρ_c	Carbon dioxide density
ρ_v	Water vapor density
ρ_w	Water density
P	Mean precipitation
Q_A	Net horizontal heat flux into or out of the water column
Q_B	Heat flux through the bottom sediments of the Reservoir
q'	Specific humidity fluctuation
RBR	Ross Barnett Reservoir
REBS	Radiation and Energy Balance Systems
Res	Surface energy budget residual, calculated as the residual of Rn – H – LE
RH	Relative humidity
Rn	Net radiation
R^2	Linear correlation coefficient
So	Incoming solar radiation
τ	Reynolds stress
T	Annual mean temperature
T_s	Sonic temperature
T_0	Water surface skin temperature
T_a	Atmospheric temperature
T_w	Water surface layer temperature
ΔT	$\Delta T = T_w - T_a$, vertical gradient of temperature over the water surface
T_{wi}	The i^{th} water temperature profile measurements
$\overline{\Delta T_{wi}}$	Mean water temperature change at the i^{th} layer over the period Δt
ΔQ_s	Change in heat storage within the water column
u, v, w	Turbulent fluctuations of wind velocity components
U	Wind speed
WD	Wind direction
μ	Molar mass ratio of dry air to water vapor
u_*	Friction velocity (m s^{-1})
z_{wi}	Water depth for the i^{th} layer
z/L	Stability parameter, z: the measurement height, L: Monin-Obukhov length
σ	Ratio of mean water vapor density to dry air density

1. Introduction

Inland fresh waters (e.g., lakes, reservoirs, wetlands, etc) compose a large portion of the land surface [*Bonan*, 1995]. These water bodies have unique characteristics in albedo, heat capacity, and roughness; and they behave differently from surrounding lands in terms of exchanges of radiation, energy, water vapor, and trace gases between the surface and the overlying atmosphere [*Bonan*, 1995; *Eaton et al.*, 2001; *MacIntyre et al.*, 2006; *Magnuson et al.*, 2000; *Walter et al.*, 2006]. Previous studies suggest that inland water bodies can exert significant influences on climate in regions where they are abundant and important [*Bates et al.*, 1995; *Blanken et al.*, 2003; *Bonan*, 1995; *Cole et al.*, 2007; *Eaton et al.*, 2001; *Long et al.*, 2007; *Rouse et al.*, 2005]. For example, based on measurements, it was estimated that including water bodies in the central Mackenzie River basin of western Canada region substantially increased regional net radiation (Rn), the maximum regional subsurface heat storage, and latent heat fluxes (LE), but substantially decreased sensible heat fluxes (H) [*Rouse et al.*, 2005]. It was also reported that the presence of the Great Lakes in general circulation model (GCM) cases resulted in a phase shift in the annual cycle of LE and H, as opposed to land [*Lofgren*, 1997].

It is projected that global hydrologic cycles will be intensified as a result of global warming and, in turn, they promote warming via the positive water vapor-temperature feedback [*Huntington*,

2006; *Solomon et al.*, 2007]. The surface energy budget over open inland waters should be used as a protocol in detecting climate change, since it is not complicated by adaptive physiological responses of terrestrial vegetation [*Blanken et al.*, 2000]. The integrated response of large inland waters to climate variability and seasonal perturbations through the large surface area and volume of water would provide a robust indicator as to whether global warming has the potential to accelerate the energy and water vapor (and thus evaporation) exchange between inland waters and the atmosphere. Thus direct measurements of the surface energy budget over inland waters are required so as to better understand the impacts of climate change or climate variability on the evaporation and hydrologic cycles [*Blanken et al.*, 2000; *Oswald and Rouse*, 2004]. Implications of changes in the surface energy budget in response to climate change are also of major significance for the local water resource management through the process of evaporation since evaporation is proportional to LE. In addition, the improvement of regional climate models for regions with inland water bodies requires details in the water surface-atmosphere interaction mechanism. In situ observations made at large inland waters would provide robust verification tools for regional climate models [*Long et al.*, 2007].

The large inland water responds to atmospheric forcings significantly differently from the surrounding lands [*Bonan*, 1995; *Eaton et al.*, 2001]. At the water surface, shortwave radiation that is not reflected back to the atmosphere may penetrate to deeper layers and is directly

absorbed by the water. The amount of solar radiation absorbed by water exponentially decreases with depth and is dependent on water turbidity, which is influenced by suspended organic and inorganic materials [*Hendersonsellers*, 1986; *Hostetler and Bartlein*, 1990]. In addition to heat transfer by conduction, water eddy diffusion leads to efficient heat transfer under the water surface [*Hendersonsellers*, 1986]. In contrast, the land surface absorbs and emits radiation fast due to its small heat capacity, and heat transfer in soils only relies on heat conduction for energy transfer, which is much less efficient. As a consequence, although water surfaces have slightly lower albedo than land surfaces (0.08 – 0.10 for water and 0.10 – 0.25 for lands) [*Budyko*, 1974], they exhibit different responses to the diurnal and seasonal changes in the solar radiation forcing, leading to distinct temporal variations in the surface temperature.

It is well known that H is primarily determined by the temperature difference between the water surface and the overlying atmosphere as well as the turbulent exchange coefficient, while LE is dependent upon vapor pressure differences at the water-air interface as well as upon the turbulent mixing intensity [*Bonan*, 1995; *Garratt*, 1992; *Hendersonsellers*, 1986; *Hostetler and Bartlein*, 1990; *Nordbo et al.*, 2011]. The water surface is almost always at its saturation point, and vapor pressure at the surface is a function of the water surface temperature [*Hostetler and Bartlein*, 1990], making the water surface temperature a key element in determining the water-atmosphere energy exchange. Consequently, temporal variations in H and LE are largely governed by

variations in the water surface temperature and the meteorological properties (e.g., wind speeds, air temperature and humidity) of over-water air masses [*Rouse et al.*, 2008; *Schertzer et al.*, 2003].

Studies of large high-latitude lakes indicate that the water stores a large amount of solar energy in the spring and summer, leading to a gradual increase in water temperature [*Rouse et al.*, 2003; *Winter et al.*, 2003]. Since the water temperature increases much more slowly than the overlying air, there is a thermal inversion, or small temperature difference, between the water surface and the overlying atmosphere. During this heating stage, H and LE are usually dampened due to the presence of the stably stratified atmospheric surface layer (ASL) [*Oswald and Rouse*, 2004]. As the seasons progress into the fall and winter—when the absorbed solar radiation is small—the air temperature decreases at a faster rate and becomes lower than the water temperature, leading to a large positive temperature gradient and an unstable ASL. It is expected that evaporation usually occurs during this period, since continental air masses in the ASL are almost always drier than the water-air interface, where water vapor pressure is nearly at saturation, producing positive vapor pressure gradients in the ASL [*Blanken et al.*, 2003; *Lenters et al.*, 2005]. In some cases, however, condensation may occur when warm and humid air masses pass over water which is cold enough to make the vapor pressure of the air masses greater than the saturation pressure in the water-air interface [*Blanken et al.*, 2000; *Liu et al.*, 2009].

As long as mechanical turbulence mixing is sufficient, H and LE (and thus evaporation) are promoted when the ASL is unstable, and depressed when the ASL is stable. In the wintertime, when net radiation (Rn) is small, H and LE are still substantial. This energetic exchange of sensible and latent heat between the water surface and the atmosphere is fueled by the energy previously stored in the water, acting as an energy source [*Rouse et al.*, 2005]. It remains unclear whether these observed physical processes that govern energy and moisture exchanges between large northern high-latitude lakes and the atmosphere are applicable to mid- and low-latitude inland waters [*Sacks et al.*, 1994; *Vallet-Coulomb et al.*, 2001].

Previous efforts have also focused on studying the significant intraseasonal variations that are strongly associated with synoptic weather events and strong wind activities [*Blanken et al.*, 2003; *Blanken et al.*, 2000; *Lenters et al.*, 2005; *Liu et al.*, 2009; *Rouse et al.*, 2003]. For instance, it was found in the Great Slave Lake that for its ice-free season, more than 50% of the measured evaporation occurred over only 25% and 20% of the days for the studied two years, in association with the passages of cold, dry air masses over the lake. These passages of cold, dry air masses led to large H and LE events which contributed to substantial increases in evaporation in high-latitude lakes (e.g., [*Blanken et al.*, 2003; *Lenters et al.*, 2005]). These large H and LE events (pulses) were also present over a large southern reservoir, occurring during 26% of the

days in the cool season and increasing the seasonal H by 42% and LE by 157%, respectively [*Liu et al.*, 2009]. These large H and LE events were also associated with cold front activities in this region [*Liu et al.*, 2009], and contributed to differences in the surface energy budget between two cool seasons due to changes in frequency, duration, and intensity of the events [*Liu et al.*, 2011]. It has not been studied yet as to whether different synoptic weather activities between two years affect interannual variations in the water surface energy budget and evaporation rates.

Although these previous studies provide useful analyses on the water-atmosphere interactions, particularly in high latitudes, there is still a lack of direct, long-term measurements of the water surface budget over mid- to low-latitude regions. In this study, we report eddy covariance measurements and analyses of the surface energy budget over the Ross Barnett Reservoir, a large inland water in central Mississippi, over the course of 2008 and 2009. This study will contribute to knowledge gained from others that use the eddy covariance technique for longer-term measurements of the surface energy budget over water in high-latitudes [*Blanken et al.*, 2008; *Blanken et al.*, 2000; *Nordbo et al.*, 2011; *Vesala et al.*, 2006]. The objectives of this study are to quantify seasonal, diurnal, and interannual variations in the surface energy budget and analyze the mechanisms that control H and LE on these timescales.

2. Methods

2.1 Site description

Ross Barnett Reservoir is located in central Mississippi (32°26'N, 90°02'W), serving as the state's largest drinking water resource (Figure 1). It is fed by the Pearl River from the northeast, and discharges into a river in the south through a 3.5-mile man-made dam and spillway. On average, the reservoir has a surface area of about 33,000 acres (130 km^2) and the water depth varies from 4 to 8 m. The water elevation is 90.7 m above sea level in summer and 90.2 m in winter.

A stationary wood platform was constructed and located in the south center of Ross Barnett Reservoir. It had a deck area of 3 m × 3 m and was approximately 1.6 m above the water surface when it was initially built in August of 2007. The water around the platform was 5 m in depth on average. A 5 m tower (Climatronics Corp.) was installed and mounted over the platform (Figure 1). The distance from the tower to shore ranged from 2.0 km to more than 10 km to minimize the footprint influences on fluxes from the surrounding lands (Figure 1).

Ross Barnett Reservoir
(32°26' N, 90°02' W)

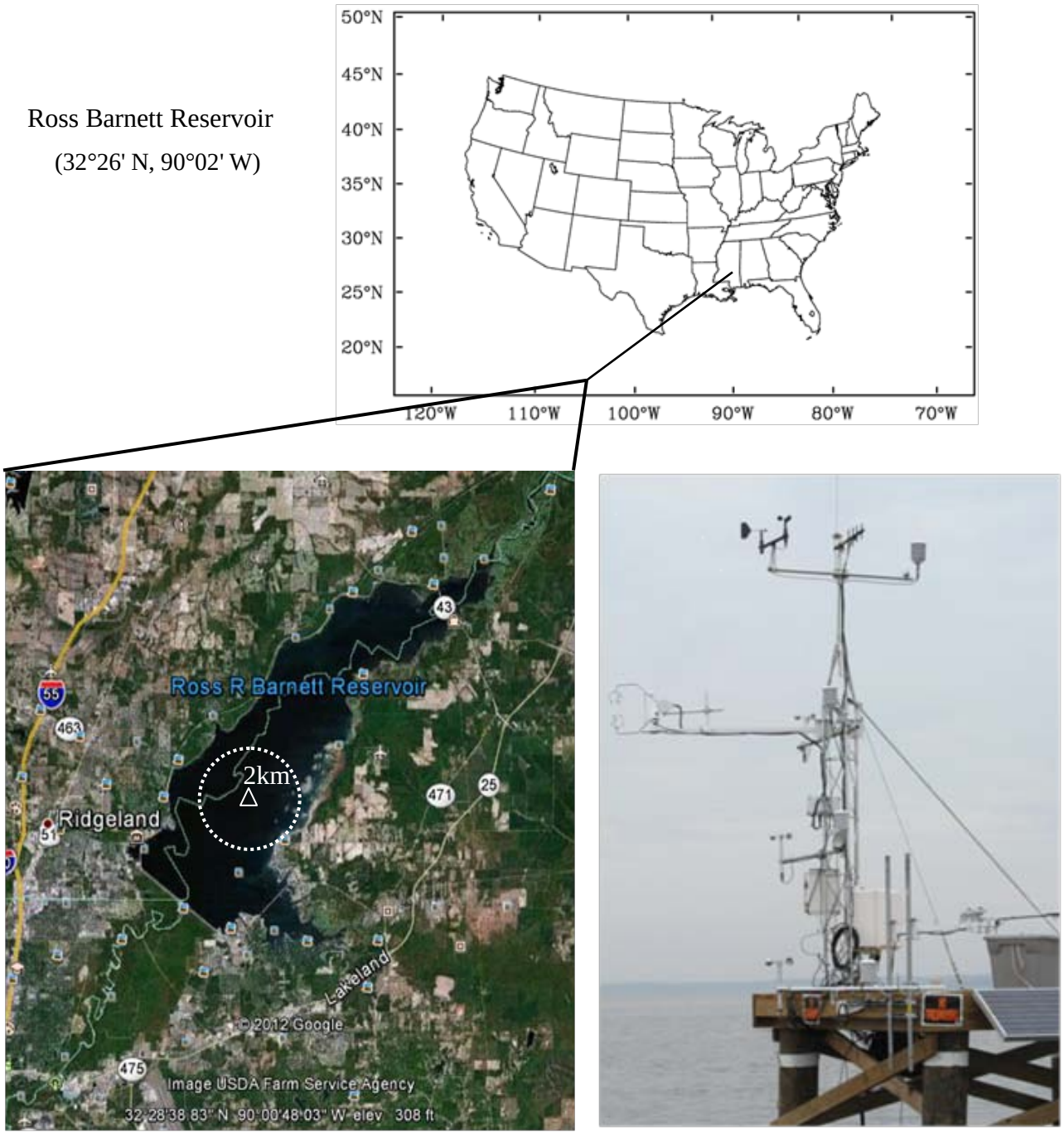

Figure 1. Location of the study site in Ross Barnett Reservoir, Ridgeland, Mississippi (Google 2012). Triangle in the bottom left panel denotes the tower location (32.43823°N, 90.03168°W)

2.2 The surface energy balance over water

The surface energy budget for the water surface may be represented through Eq. (1) and its schematic view is shown in Figure 2.

$$Rn - H - LE - G - K_p = 0 \qquad (1)$$

where Rn denotes the net radiation measured at the water surface (positive for absorption by the surface); K_p is the solar radiation that penetrates through the water surface into the deeper layers; H is the positive sensible heat flux out of the surface; LE is the positive latent heat flux out of the surface; G represents the downward heat flux which is transferred by both molecular conduction and large eddy diffusion from the water surface to the deeper layers (all energy terms expressed in W m^{-2}).

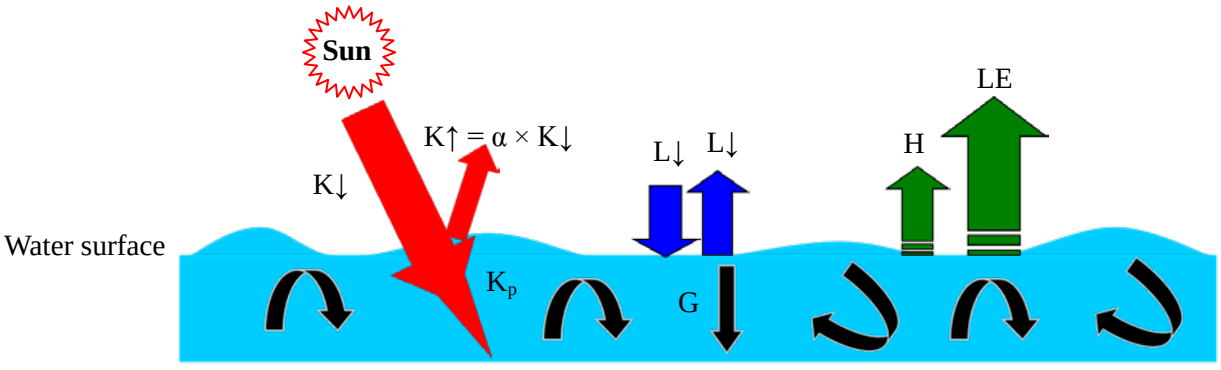

Figure 2. Schematic view of the water surface energy balance. K↓: incident shortwave radiation, K↑: reflected shortwave radiation, α: albedo, Kp: penetrating shortwave radiation, L↓: incoming longwave radiation; L↑: outgoing longwave radiation, H: sensible heat flux, LE: latent heat flux, G: water heat flux.

Specifically, the net radiation absorbed by the water surface ($Rn - K_P$) is the net result of incoming solar radiation (K↓), reflected solar radiation (K↑), incoming long-wave radiation (L↓) and outgoing long-wave radiation (L↑), and, as described by

$$Rn - K_p = K\downarrow - K\uparrow + L\downarrow - L\uparrow \quad (2)$$

For the water column below the water surface down to the water-sediment interface, the energy balance can be described by

$$K_p + G = Q_B + Q_A + \Delta Q_S \quad (3)$$

where Q_B is the heat flux through the bottom sediments of the Reservoir, Q_A is the net horizontal heat flux brought by horizontal water currents into or out of the water column, ΔQ_S is the change in heat storage within the water column (positive for warming) and can be quantified by change in water temperatures, as

$$\Delta Q_S = \frac{\rho_w C_{pw} \sum_{i=1}^{n} \Delta \overline{T_{wi}} z_{wi}}{\Delta t} \quad (4)$$

where ρ_w is the density of water (kg m^{-3}), C_{pw} is the specific heat of water (J °C·kg^{-1}), z_{wi} is water depth (m) for i^{th} layer where the i^{th} water temperature profile measurements (T_{wi}; °C) were made (n = 8 in this study). Therefore, $\Delta \overline{T_{wi}}$ is the mean water temperature change at the i^{th} layer over the period Δt.

Previous studies indicated that Q_B can be neglected because it only contributes less than 5% of

the heat storage change in lakes [*Stannard and Rosenberry*, 1991; *Sturrock et al.*, 1992]. Q_A is negligible for water bodies with small inflow and outflow volumes, which is particularly true for this reservoir. It was found that large errors can be induced in determining ΔQ_S (based on Eq. (4)) due to localized changes in water temperatures by water eddy diffusion, thus the energy budget residual (Res) is widely applied to obtain ΔQ_S, based on Equations (1), (2) and (3) [*Blanken et al.*, 2003; *Lenters et al.*, 2005; *Nordbo et al.*, 2011].

$$\Delta Q_S = \mathrm{Re}\, s = Rn - H - LE \qquad (5)$$

This study will used Eq. (5) to estimate ΔQ_S in particular because of the lack of high quality surface water temperatures (as explained in more detail later).

2.3 Instruments

In this study, an eddy covariance system was mounted 4 m above the water surface, including a three-dimensional sonic anemometer (model CSAT3, Campbell Scientific, Inc.) and an open path CO_2/H_2O infrared gas analyzer (IRGA; Model LI-7500, LI-COR, Inc.). The sonic anemometer measured turbulent fluctuations of wind velocity components (u, v, and w) and fluctuations of sonic temperature (T_s). The IRGA measured fluctuations of densities of carbon dioxide (ρ_c) and water vapor (ρ_v). The horizontal distance between the sonic anemometer and the IRGA was approximately 20 cm. Signals from the eddy covariance sensors were recorded at a frequency of

10 Hz by a datalogger (model CR5000, Campbell Scientific, Inc.). The turbulent fluxes of sensible heat, latent heat and momentum in kinematic forms can be quantified as the 30-min mean covariance between w' and c', where c is respective quantity as

$$\widetilde{H} = \overline{w' T_S'} \tag{6}$$

$$\widetilde{LE} = \overline{w' \rho_v'} \tag{7}$$

$$\left|\widetilde{\tau}_{\text{Re}\,ynolds}\right| = \rho_a \sqrt{(\overline{u'w'})^2 + (\overline{v'w'})^2} \tag{8}$$

For each variable the prime in the above equations represents instantaneous departures from its 30-min mean. We also measured a variety of meteorological variables as 30-min averages of 1 s readings.

Net radiation (Rn) was measured using a net radiometer (model Q-7.1, Radiation and Energy Balance Systems (REBS), Campbell Scientific, Inc.). It was mounted approximately 1.2 m above the water surface. Incoming solar radiation was measured with a silicon pyranometer (model LI-200, LI-COR, Inc.). Air temperature (T_a) and relative humidity (RH) were measured using temperature and humidity probes with 10-plate radiation shields (model HMP45C, Vaisala, Inc.) on the tower at approximately 1.9, 3.0, 4.0, and 5.46 m above the water surface. Wind speeds (U) and wind direction (WD) were measured using a wind sentry unit (model 03001, RM Young, Inc.) at 5.46 m. Three other wind speed sensors (model 03101, RM Young, Inc.) were mounted at heights of 1.9, 3.0, and 4.0 m above the water surface with the HMP45C humidity probes.

Water surface temperature (T_0) was measured using an infrared temperature sensor (model IRR-P, Apogee, Inc.). T_0 was not used in this study due to the malfunction of the infrared temperature sensor since the beginning of 2009. The water temperature profile was measured by temperature sensors (model 107-L, Campbell Scientific, Inc.) which were attached to a buoy and placed at depths of 0.10, 0.25, 0.5, 1.0, 1.5, 2.5, 3.5, and 4.5 m below the water surface. The water temperature measured at 0.5 m depth was used to represent the water surface layer temperature (T_w) for this study. Vapor pressure (e_w) at the water surface was estimated by calculating the saturation vapor pressure at the water surface layer temperature (T_w). Precipitation was measured using a tipping bucket rain gauge to obtain 30-min accumulative precipitation rates (model TE525, Texas Instruments, Inc.). Table 1 lists all of the instruments used in this study and their corresponding measurement heights.

Two solar panels (model SP65, 65 Watt Solar Panel, Campbell Scientific, Inc.) were mounted on the platform to charge six deep cycling marine batteries and provide power for all the instruments. All slow-response sensor signals were also recorded with the CR5000 datalogger at 30-min intervals. The 30-min average data were accessed from shore through a wireless radio system (model FGR-115RC, FreeWave 900 MHz Spread Spectrum Radio, 1 Watt, FreeWave Technology, Inc.). The instruments were checked and maintained and the 30-min time-series data were downloaded on a monthly basis.

Table 1. List of the instruments for fast-response (10 Hz) and for slow-response (1 s) used in this study.

Instruments	Variables	Model and maker	Heights/Depths (m)
	Fast-response variables measured at 10 Hz		
Three-dimensional sonic anemometer	u, v, w, T_s	model CSAT3, Campbell Scientific, Inc.	4.0
Open path CO_2/H_2O infrared gas analyzer	ρ_v, ρ_c	model LI-7500, LI-COR, Inc.	4.0
	Slow-response variables measured at 1 s		
Net radiometer	Net radiation (Rn)	model Q-7.1, Campbell Scientific, Inc.	1.2
Silicon pyranometer	Incoming solar radiation (So)	model LI-200, LI-COR Inc.	1.2
Temperature and humidity probe	Air temperature (T_a) Relative humidity (RH)	model HMP45C, Vaisala, Inc.	1.9, 3.0, 4.0, and 5.46
Wind sentry unit	Wind speed (U) and wind direction (WD)	model 03001, RM Young, Inc.	5.46
Wind speed sensor	Wind speed (U_i)	model 03101, RM Young, Inc.	1.9, 3.0, and 4.0
Infrared temperature sensor	Water surface temperature (T_0)	model IRR-P, Apogee, Inc.	-
Temperature sensor	Water temperature (T_w)	model 107-L, Campbell Scientific, Inc.	0.10, 0.25, 0.5, 1.0, 1.5, 2.5, 3.5, and 4.5
Tipping bucket rain gauge	Precipitation	model TE525, Texas Instruments, Inc.	-

A summary of the 30-min data and their availability is listed in Table 2. Considering all missing and rejected data, data availability was good in 2008, with around 95% available data points for each measured variable. In 2009, S_o (incoming solar radiation), Rn, T_a, T_w and RH were of good quality with around 93% available data points, while the percentage for available H, LE, and wind speed data points were only 80%, 80%, and 87%. Note that data gaps were caused by instrument failures, calibrations, and precipitation, especially for H and LE.

Table 2. Summary of 30-min data and their availability in 2008 and 2009. Data gaps were caused by instrument failures, calibrations, and precipitation.

Variable	Unit	Year	Mean	Max	Min	Stdev	Data points (%)
So	W m^{-2}	2008	181.5	977.9	0.0	265.2	93.2
		2009	172.2	952.5	0.0	283.0	93.2
Rn	W m^{-2}	2008	110.7	929.6	-162.1	250.8	97.3
		2009	105.4	903.4	-128.5	243.1	93.6
H	W m^{-2}	2008	17.2	222.6	-151.4	34.3	96.1
		2009	14.9	258.9	-99.8	30.1	80.3
LE	W m^{-2}	2008	89.1	523.4	-131.0	75.1	95.9
		2009	78.6	575.9	-93.3	68.4	80.0
T_a	ºC	2008	18.0	35.3	–6.0	8.1	97.3
		2009	18.0	35.8	–5.3	8.1	93.6
T_w	ºC	2008	20.6	34.4	7.0	7.4	94.8
		2009	20.2	35.0	6.4	7.6	93.2
U	m s^{-1}	2008	3.6	24.5	0.2	2.5	97.3
		2009	3.1	11.7	0.2	2.0	87.0
RH	%	2008	69.9	100.0	22.2	15.8	97.3
		2009	69.2	100.0	20.7	15.9	93.6
Major data gaps	month (days)	2008	Feb (4) and Dec (11)				
		2009	Jan (4), Mar (5), May (13), Jun (5), Aug (4), Sep (11), Oct (17) and Dec (12)				

2.4 Postfield processing of eddy covariance data

Raw time-series turbulence data collected in this study were processed and corrected to obtain eddy covariance fluxes, using a postfield data processing program [*Liu et al.*, 2005]. This program was used in the energy balance experiment (EBEX) [*Mauder et al.*, 2006], and has been updated following recommendations by Mauder and Foken [2004] since then [*Liu et al.*, 2009]. The following data processing steps were performed.

1. Despiking: Data spikes in eddy covariance systems may be caused by random electronic spikes in the instruments or by precipitation collecting on sonic transducers or the window of gas analyzers [*Vickers and Mahrt*, 1997]. The despiking routine developed by Hojstrup [1993] has been widely used in the flux community and therefore was followed in this study [e.g., *Foken et al.*, 2012]. To apply this method, the mean and standard deviation for a series of moving windows with a certain window length was first computed. The window moved forward one value at a time. Any value exceeding several times its standard deviations was considered a spike, unless four or more consecutive points were detected, in which case the "spike" was considered to be physical. Spikes were then replaced by linear interpolation. We took the window length to be 10 (corresponding to 1 second), as in *Hojstrup* [1993] and *Mauder and Foken* [2004]. We used a value of 5.5 times the standard deviations in our calculation, as suggested by *Vickers and*

Mahrt [1997].

2. Coordinate Rotation: We used the double rotation for rotating the coordinate system for each averaging period (i.e., 30 minutes in this study). First the x-y plane was rotated at angle α about the z-axis such that:

$$\alpha = \tan^{-1}\left(\frac{\bar{v}}{\bar{u}}\right) \tag{9}$$

The new x-z plane was then rotated at angle β such that:

$$\beta = \tan^{-1}\left(\frac{\bar{w}}{\sqrt{\bar{u}^2 + \bar{v}^2}}\right) \tag{10}$$

After the two rotations, we obtained $\bar{v} = \bar{w} = 0$.

3. Block Averaging: We used 30 minute block averaging to obtain the means for time-series data, which were then removed from the raw data to get the fluctuating quantities for further calculations. Note that the calculated mean fluxes are affected by the choice of averaging period. Short averaging periods lead to a loss of the low frequency contributions to the fluxes, while long averaging periods the steady state condition may not be fulfilled. The 30 min block averaging is recommended to use over the whole day [*Foken*, 2008]. However, it has been shown that the 30 min block averaging underestimates the fluxes by 4-17% [*Finnigan et al.*, 2003; *Sakai et al.*, 2001].

4. Flux Calculations: Preliminary sensible, latent and momentum fluxes in kinematic form were first calculated using Eqs. (6), (7), and (8), respectively. Since we did not use a fine wire thermocouple in the eddy covariance system for temperature measurements, the sonic temperature was used for calculating sensible heat flux (Eq. (6)). Because the speed of sound is dependent on humidity in addition to temperature, heat flux from Eq. (6) must be corrected for the effect of moisture fluxes. This correction is discussed in detail in step 6.

5. Webb Pearman and Leuning (WPL) Corrections: Due to the density effects, latent heat fluxes obtained by Eq. (7) must be corrected according to WPL corrections [*Webb et al.*, 1980]. When the temperature and humidity fluctuations are known, the latent heat flux after WPL corrections can be obtained as

$$\overline{w'\rho'_{vc}} = (1+\mu\sigma)\left[\overline{w'\rho'_v} + (\frac{\overline{\rho_v}}{\overline{T}})\overline{w'T'}\right] \qquad (11)$$

where μ is the molar mass ratio of dry air to water vapor, and σ is the ratio of mean water vapor density to dry air density.

6. Sonic Temperature Correction: Sonic anemometers derive temperature measurements from the speed of sound in air, which is affected by crosswind and changes in humidity [*Liu et al.*, 2001;

Schotanus et al., 1983]. However, crosswind corrections were made internally in the CSAT3 sonic anemometer (Campbell Scientific Inc.). Therefore, sensible heat fluxes obtained by Eq. (6) must be corrected for humidity fluctuations by:

$$\overline{w'T'_{sc}} = \overline{w'T'_s} - 0.51 \cdot \overline{T} \cdot \overline{w'q'} \quad (12)$$

where q' is the specific humidity fluctuation and $\overline{T}$ is the average air temperature which was measured by a HMP45C in this study.

7. Convergence Test: It can be seen in steps 4, 5, and 6 that the sensible and latent heat fluxes were interdependent. Therefore, steps 4-6 were typically iterated until the difference in fluxes between iterations was 0.01% or less [*Mauder and Foken*, 2004], yielding sensible (H) and latent (LE) heat fluxes reported in this study;

$$H = \rho_a C_p \cdot \overline{w'T'_{sc}} \quad (13)$$

$$LE = L \cdot \overline{w'\rho'_{vc}} \quad (14)$$

where ρ_a is the air density, C_p is the specific heat of air, and L is the latent heat of vaporization. Additionally, friction velocity (u_*) reported in this study was defined by the relation

$$u_*^{\,2} = \frac{\left|\tau_{Reynolds}\right|}{\rho_a} \quad (15)$$

where τ is the Reynolds stress and ρ_a is the air density.

3. Results and discussion

3.1 General climate

3.1.1 Temperature and precipitation

Mississippi is located in the subtropical zone, with short mild winters and long, hot and humid summers. The data from a climate monitoring station at the Jackson International Airport, 15 km southeast of the study site, indicate that the 47-year mean air temperature and precipitation from 1964 to 2010 were 18.2˚C and 1,398 mm, respectively (Figure 3; National Climatic Data Center, http://www.ncdc.noaa.gov/oa/ncdc.html). The temperature records show that the Jackson area has been warming at a rate of 0.13C per dec ade during the past 47 years. No statistically significant trend was found for the precipitation.

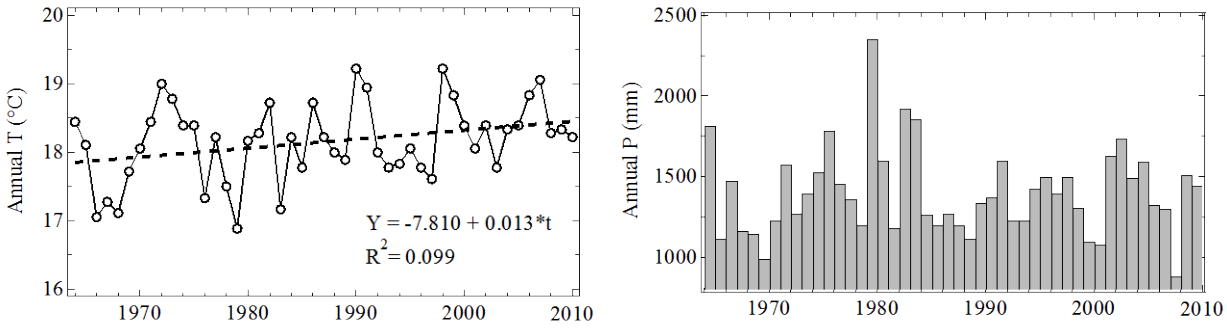

Figure 3. Annual mean temperature (T) and precipitation (P) from 1964 to 2010 at the Jackson International Airport, Mississippi. Figure on the left shows the 0.13˚C per decade warming trend for this area during the last 47 years.

Both the annual mean air temperatures for 2008 and 2009 were 18.3˚C and slightly above the 47-year mean of 18.2˚C. There was slightly more precipitation in 2008 (1,514 mm) than in 2009 (1,442 mm). Monthly mean temperatures showed similar patterns in 2008 and 2009 (Figure 4, Table 3). Temperatures increased from 7.3˚C (8.6˚C) in January to 28.3˚C in July (27.6˚C in June), and decreased to 10.1˚C (7.6˚C) in December for 2008 (2009). Precipitation showed no particular patterns and was unevenly distributed throughout the years.

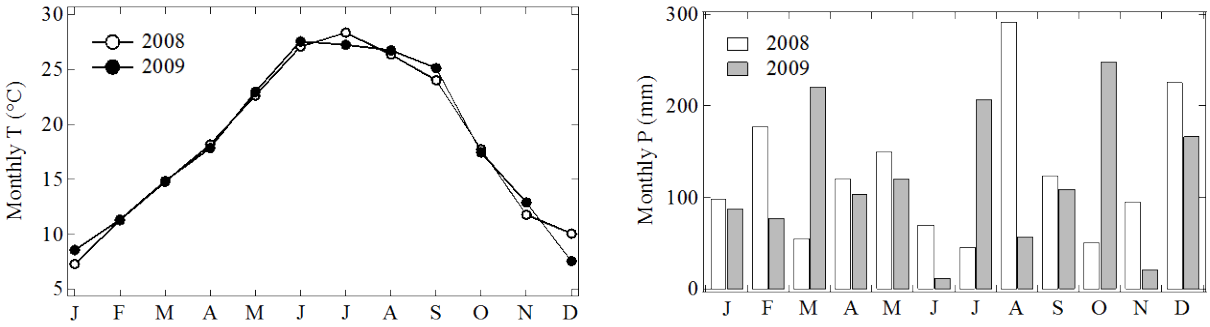

Figure 4. Monthly mean temperature (T) and precipitation (P) at the Jackson International Airport

Table 3. Monthly mean temperature (T) and precipitation (P) at the Jackson International Airport

	Month	Jan	Feb	Mar	Apr	May	Jun	Jul	Aug	Sep	Oct	Nov	Dec	Average
2008	**T** (˚C)	7.3	11.3	14.8	18.2	22.6	27.1	28.3	26.3	24	17.7	11.8	10.1	18.3
	P (mm)	99	179	56	121	151	71	46	292	124	52	96	226	1514
2009	**T** (˚C)	8.6	11.3	14.8	17.8	22.9	27.6	27.2	26.7	25.1	17.4	12.9	7.6	18.3
	P (mm)	89	78	221	105	121	13	208	58	110	249	23	167	1442

3.1.2 Synoptic weather patterns

Throughout a year, this region is under the alternate influences of anti-cyclonic and cyclonic weather systems, bringing in air masses originating from different sources [*Liu et al.*, 2009]. In the warm season (defined in this study as months from April to September), the Bermuda high circulates warm, humid air northward from the Gulf of Mexico into the southeast. In the cool season (defined in this study as months from October to March), the Canadian high dominates over North America, bringing north and northwestern cold, dry air masses into the south, accompanied by occasional cold front events [*Ahrens*, 2011]. We hypothesize that

1) *seasonal shifts in synoptic weather patterns, which lead to changes in meteorological conditions of air masses, significantly govern seasonal variations in the water surface energy budget and evaporation; and*

2) *year-to-year variations in synoptic weather events are partly responsible for interannual variations in the water surface energy budget and evaporation.*

3.2 General characteristics of the surface energy budget in 2008 and 2009

The half-hourly time series data and daily means of Rn, H, LE, and the energy budget residual (Res = Rn – H – LE) are shown in Figures 5, 6, and 7. Rn exhibited clear diurnal cycles with positive values in the daytime and negative ones at night (Figure 5). Over the two years, the daytime maximum 30-min Rn ranged from about 400 W m^{-2} in January to about 800 W m^{-2} in July, and the nighttime 30-min Rn ranged from about –150 to 50 W m^{-2}, resulting in daily means from –50 to 250 W m^{-2} (Figures 5, 7). Positive 30-min Rn occurred occasionally at nights due to warm air mass movements over this region, leading to a temperature inversion above the water surface and thus larger incoming longwave radiation than outgoing longwave radiation.

H and LE also had clear intraseasonal variations in response to short-term variations in meteorological forcings (e.g., temperature, humidity, wind speeds, etc.) (Figure 5). H was relatively small in the warm season and large in the cool season, while LE was large in the warm season and relatively small in the cool season. On a few occasions, daily mean H reached a maximum of 150 W m^{-2} or a minimum of –50 W m^{-2} (Figure 7). By contrast, LE ranged in its daily means from about –100 W m^{-2} to 400 W m^{-2} in the cool season and from –50 W m^{-2} to more than 500 W m^{-2} in the warm season. Negative LE seldom occurred in the warm season and occasionally in the cool season due to the moist air masses passing over the water surface.

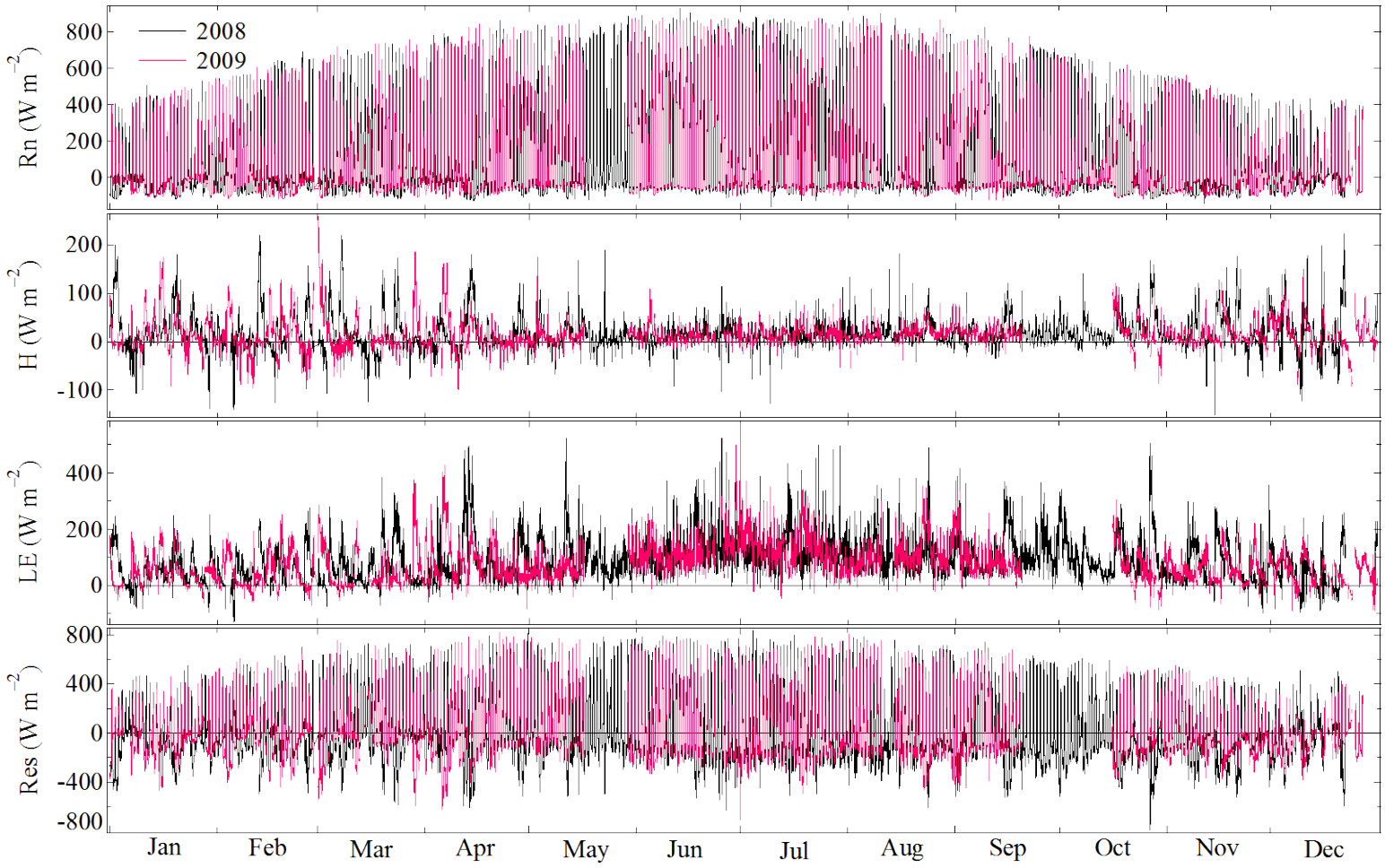

Figure 5. Half-hourly means of the energy fluxes in 2008 and 2009; Rn: net radiation, H: sensible heat fluxes, LE: latent heat fluxes, and Res: energy budget residual (Res = Rn – H – LE). Data gaps were caused by instrument failures, calibrations, and precipitation.

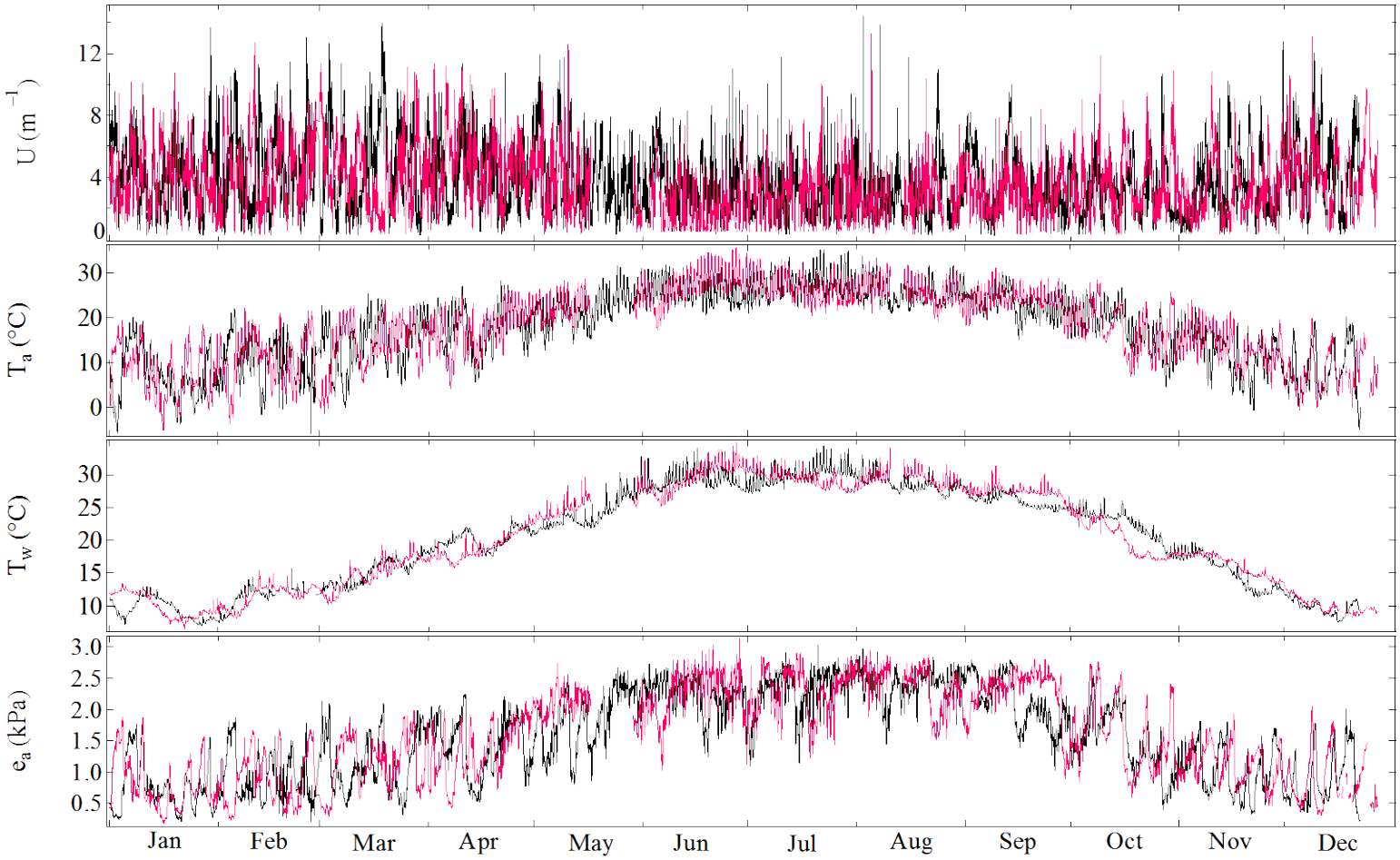

Figure 6. Half-hourly means of meteorological variables in 2008 and 2009; U: wind speeds, T_a: air temperature, T_w: water temperature, and e_a: vapor pressure. Data gaps were caused by instrument failures, calibrations, and precipitation.

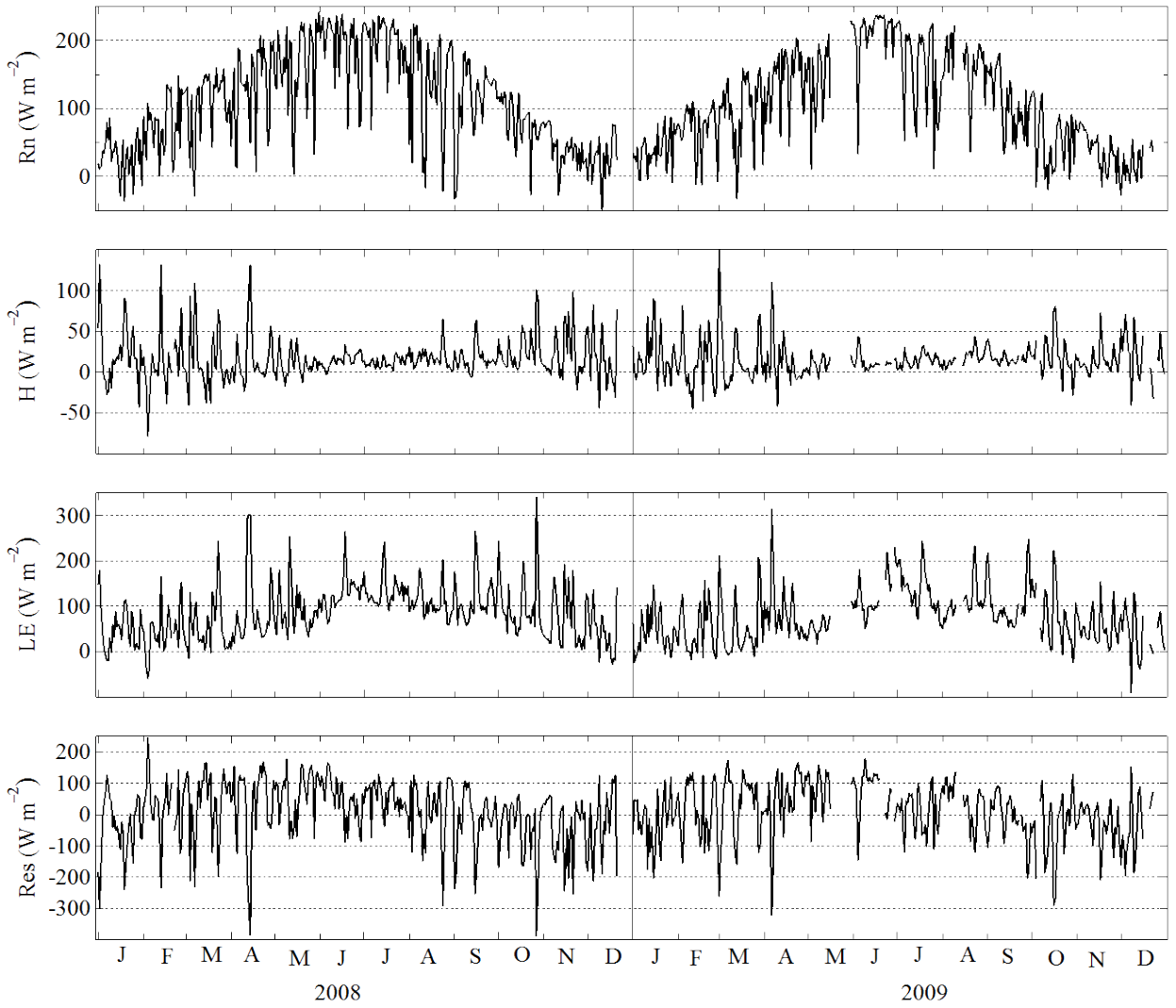

Figure 7. Daily means of the components of the surface energy budget for 2008 and 2009. Data gaps were caused by instrument failures, calibrations, and precipitation.

The energy balance closure (EBC, %) was analyzed based on the available data in 2008 followed the method of Nordbo et al. (2011). The monthly EBC varied between 85% and 117% and the annual mean was 97%. The EBC were greater than 100% (i.e., ranging from 103% to 117%) from February to June and less than 100% for the rest of the months. Particularly, the lowest EBC values occurred in November (88%), December (85%), and January (87%).

It is noted that the diurnal and even intraseasonal variations of H and LE were characterized by occasionally large H and LE pulses that were evident throughout the two years (Figures 5, 7). These H and LE pulses are distinguished by large, positive H and LE magnitudes that persisted for up to a few days. Additionally, the signatures of the diurnal variations in H and LE were diluted and superimposed with these H and LE pulses. In general, H and LE pulses occurred more often in the cool season than in the warm season. It is apparent that H (LE) pulses had larger (smaller) magnitudes in the cool season than the warm season. Further analysis indicated that these H and LE pulses were associated with high-wind events that corresponded to large wind speeds (U) as the direct consequence of a synoptic weather event. Previous studies at this site for a cool season indicated that these high-wind events (i.e., U spikes in Figure 6) were usually associated with cold, dry air masses immediately behind cold fronts, which created large vertical gradients of temperature and vapor pressure (i.e., large $T_w - T_a$ and $e_w - e_a$ in Figure 6) in the ASL [*Liu et al.*, 2009]. Strong mechanical mixing and the enhanced convective atmospheric surface layer (ASL) promoted turbulent exchanges of sensible and latent heat, generating episodic H and LE pulses [*Blanken et al.*, 2000; *Lenters et al.*, 2005; *Liu et al.*, 2009]. We hypothesize that these strong intraseasonal variations in H and LE pulses significantly contributed to the seasonal variations in the surface energy budget and also contributed to the interannual variations in the surface energy budget.

Given the substantial variability in the surface energy budget on each of these three timescales, we focused our analyses on the (1) seasonal, (2) diurnal, (3) interannual variations of the surface energy budget, as well as the impacts of H and LE pulses on the surface energy budget. The controlling factors for the surface energy budget on each timescale were also examined. The objectives for such analyses were to investigate physical processes and mechanisms that regulate diurnal, seasonal, and interannual variations in the surface energy budget over a southern inland water surface. We then compared our results with studies over other regions, aiming to examine applicability of our conclusions obtained over this low-latitude inland water in other geographical locations.

3.3 Seasonal variations

3.3.1 General seasonal variations in the surface energy budget

The general features of Rn, H, and LE on the seasonal scale can be analyzed through their half-monthly means over the course of the years (Figure 8a, Table 4). On the half-monthly basis, Rn presented a clear pattern associated with solar radiation. It increased gradually from 33.4 W m^{-2} in January, reached its maximum of 204.0 W m^{-2} in June, and then leveled off afterwards to its minimum of 15.2 W m^{-2} in December. Rn remained positive throughout the year, continuously providing the primary energy input for heating water.

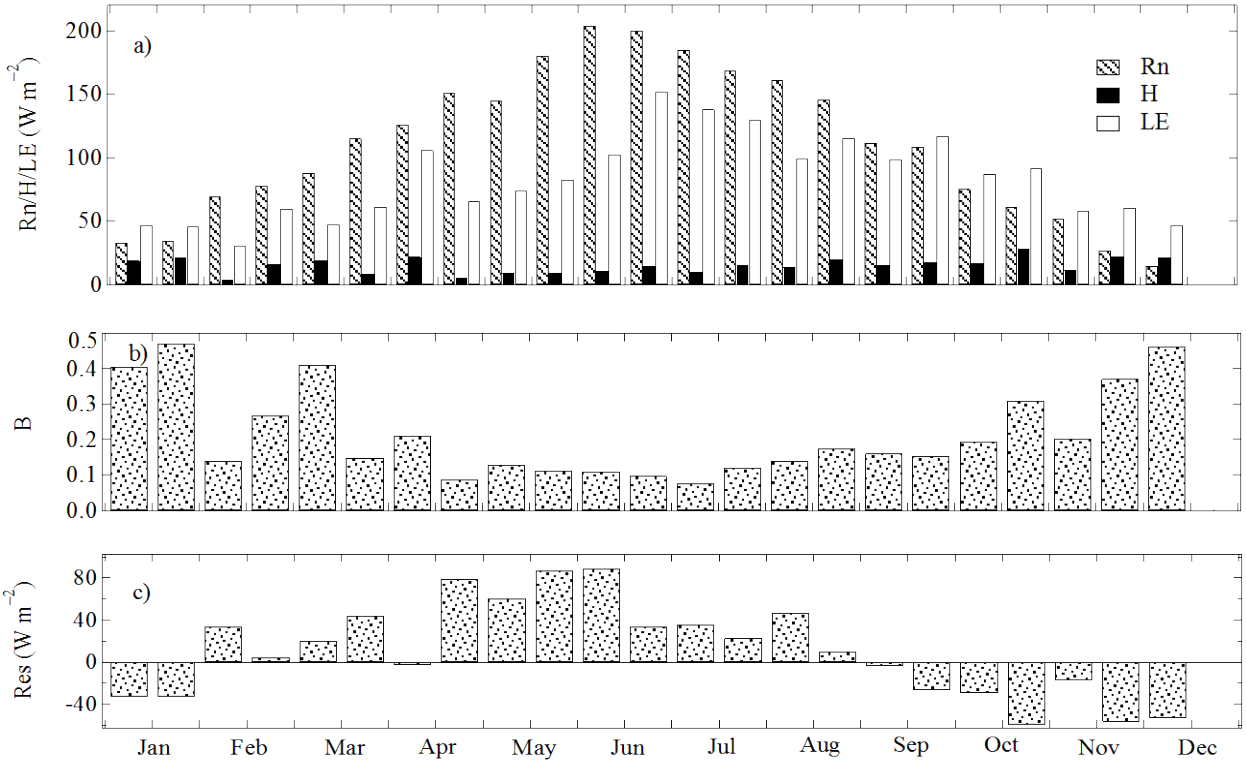

Figure 8. Two-year averaged half-monthly means of the surface energy budget: a) net radiation (Rn) and sensible (H) and latent (LE) heat fluxes, b) Bowen ratio (B), and c) the energy budget residual (Res = Rn – H – LE). Only data in the second half of May are available for 2008. The data in the second half of December for both years are not included due to large gaps in data points.

Table 4. Half-monthly averaged components of the surface energy budget and meteorological variables in 2008 and 2009. Table parameters are defined in the notes at the bottom of the table.

Month	Half	So	Rn	H	LE	Res	B	u_*	U	RH	T_a	T_w	ΔT	e_a	e_w	Δe
		W m^{-2}	W m^{-2}	W m^{-2}	W m^{-2}	W m^{-2}		m s^{-1}	m s^{-1}		°C	°C	°C	kPa	kPa	kPa
Jan	1st	104.7	33.4	19.2	47.3	–33.1	0.41	0.18	4.26	0.69	9.2	11.0	1.8	0.89	1.32	0.43
	2nd	100.5	34.9	21.6	46.0	–32.6	0.47	0.19	4.11	0.68	5.7	8.4	2.8	0.66	1.11	0.45
Feb	1st	144.5	69.6	4.4	31.0	34.2	0.14	0.18	4.34	0.66	10.9	10.7	–0.3	0.91	1.29	0.38
	2nd	142.7	78.3	16.2	60.1	5.0	0.27	0.20	4.71	0.66	10.2	12.4	1.9	0.87	1.44	0.60
Mar	1st	135.0	88.4	19.7	47.9	20.8	0.41	0.20	4.41	0.72	12.1	13.2	1.1	1.07	1.52	0.45
	2nd	191.1	115.4	9.2	61.6	44.6	0.15	0.20	4.58	0.66	15.8	16.7	1.0	1.21	1.91	0.70
Apr	1st	180.0	126.4	22.4	106.3	–2.4	0.21	0.22	4.96	0.66	16.1	18.7	2.7	1.25	2.17	0.91
	2nd	226.7	151.8	6.0	66.5	79.4	0.09	0.18	4.14	0.67	19.2	20.3	1.1	1.50	2.40	0.89
May*	1st	210.6	145.6	9.6	74.7	61.3	0.13	0.20	4.10	0.72	21.8	23.5	1.8	1.88	2.91	1.03
	2nd	247.3	180.3	9.5	82.9	87.9	0.11	0.16	3.35	0.70	23.6	25.5	1.9	2.03	3.28	1.25
Jun	1st	269.6	204.0	11.5	102.8	89.8	0.11	0.17	3.22	0.68	26.1	28.5	2.4	2.25	3.89	1.64
	2nd	270.8	200.5	15.1	152.1	34.2	0.10	0.14	3.24	0.63	27.6	30.3	2.7	2.25	4.32	2.07
Jul	1st	250.5	185.2	10.7	138.3	36.1	0.08	0.15	3.15	0.63	27.4	29.7	2.3	2.28	4.19	1.91
	2nd	233.5	169.2	15.8	130.1	23.3	0.12	0.16	3.20	0.68	26.7	29.6	2.9	2.33	4.17	1.84
Aug	1st	220.1	161.1	14.1	99.8	47.2	0.14	0.14	2.65	0.71	26.5	29.4	2.9	2.44	4.11	1.66
	2nd	211.6	146.4	20.6	115.8	10.1	0.18	0.16	3.08	0.73	25.3	28.6	3.2	2.34	3.91	1.56
Sep	1st	172.8	112.1	16.1	99.3	–3.3	0.16	0.20	3.61	0.77	24.4	27.2	2.8	2.35	3.60	1.25
	2nd	183.2	109.0	18.1	117.5	–26.3	0.15	0.14	2.91	0.73	23.0	26.1	3.2	2.05	3.39	1.34
Oct	1st	136.6	75.8	17.2	87.8	–29.1	0.20	0.17	3.26	0.77	20.5	23.4	2.9	1.85	2.88	1.04
	2nd	153.4	61.1	28.5	92.4	–59.8	0.31	0.18	3.54	0.70	14.9	19.2	4.4	1.21	2.25	1.04
Nov	1st	142.2	52.6	11.9	58.1	–17.4	0.20	0.14	2.98	0.68	15.1	17.4	2.4	1.18	1.99	0.82
	2nd	101.6	27.1	22.6	60.8	–56.4	0.37	0.16	3.47	0.71	10.9	13.8	3.0	0.96	1.59	0.63
Dec	1st	75.6	15.2	21.7	46.8	–53.4	0.46	0.21	4.62	0.73	7.7	10.3	2.6	0.82	1.26	0.43
	2nd	-	-	-	-	-	-	-	-	-	-	-	-	-	-	-
Mean		**178.5**	**110.6**	**15.7**	**83.7**	**11.3**	**0.22**	**0.18**	**3.73**	**0.69**	**18.3**	**20.6**	**2.3**	**1.59**	**2.65**	**1.06**

Notes: So: incoming solar radiation, Rn: net radiation, H: sensible heat flux, LE: latent heat flux, Res: the energy budget residual (Res = Rn – H – LE), B: Bowen ratio, u_*: friction velocity, U: wind speed, RH: relative humidity, T_a: air temperature, T_w: water temperature at 0.5 m depth, ΔT: vertical temperature gradient between the water surface and the air, e_a: vapor pressure in the atmosphere (T_w–T_a), e_w: vapor pressure at the water-air interface calculated using T_w, Δe: vertical vapor pressure gradient between water surface and the air (e_w–e_a).

H showed no correspondence to the pattern of Rn (Figure 8a). In the warm season, the half-monthly average H was relatively small and varied little, increasing gradually from the low value of 6 W m^{-2} in late April to the high value of 20.6 W m^{-2} in late August as the seasons progressed (Table 4). In the cool season, H became larger and had more variances, ranging between 4.4 W m^{-2} in late February to 28.5 W m^{-2} in late October. The largest H fluctuation occurred in February, when H decreased by 80% during the first half of February, and increased by a factor of 3.7 during the second half. Compared with the large values of Rn and LE, the generally small H indicates that only a small amount of Rn absorbed by the water was used for the sensible heating of the atmosphere.

Different from H, LE followed the seasonal variation patterns of Rn quite well. The half-monthly average LE increased from about 50 W m^{-2} in January, reached its maximum of 152.1 W m^{-2} in late June, and then decreased to about 50 W m^{-2} by December (Figure 8a, Table 4). The large values of LE indicate that a large portion of Rn absorbed by the water was utilized for evaporation. It was also observed that there was roughly a half-month time lag between maximums of Rn and LE, and LE changed at a smaller rate before and after its maximum. This suggests that LE did not respond to Rn concurrently due to the large heat capacity of the water. LE was always at least two times larger than H, as reflected by the annual mean of the ratio of H versus LE of 0.22 (Bowen ratio; Table 4; Figure 8b). The Bowen ratio was small and invariant in

the warm season (around 0.1), showing that a large portion of Rn was used to fuel evaporation; while it was large and varied substantially in the cool season, showing that relatively large amounts of energy were supplied for sensible heat exchange between the water surface and the atmosphere.

The residual of surface energy balance, Res, was used in this study to address the heat storage change in water. In general, half-monthly Res closely followed the Rn pattern. Res increased in the first half of January (–33.1 W m^{-2}), maximized in the first half of June (89.8 W m^{-2}) and decreased thereafter to its minimum in the first half of December (–53.4 W m^{-2}) (Figure 8c; Table 4). The occasional low Res in early April and high Res in November corresponded to the occurrences of large H and LE pulses. It means that the energy that was used to drive the H and LE pulses in these two months was largely supplied by the energy stored in the water. On average, the reservoir transferred from a net cooling phase to a net warming phase in early February, and reversed to net cooling phase again in late August. In the net warming phase from February to August, Res remained positive due to the larger Rn than the sum of H and LE. The excessive portion of the energy was absorbed and stored in the water. During the net cooling phase from September to January, Rn decreased at a larger rate and even became smaller than the sum of H and LE, resulting in slow releases of the previously stored energy in the water to the atmosphere through turbulent exchanges of H and LE (Figure 8; Table 4).

It is well known that Rn is one major external forcing for the surface energy exchanges [*Winter et al.*, 2003]. In our case, LE followed Rn on the seasonal scale, while H varied completely differently from Rn, clearly indicating that there were other external forcings that drove seasonal variations in H and LE. These forcings included, but were not limited to, the temperature and saturation vapor pressure of the water surface (T_w, e_w) and those of the overlying atmosphere (T_a, e_a), their vertical gradients between the water and the air ($\Delta e = e_w - e_a$, $\Delta T = T_w - T_a$), and wind speed (U). The factors controlling seasonal variations in H and LE will be analyzed in the following two subsections (3.3.2 and 3.3.3), respectively, through the two-year averaged half-monthly means throughout the year (Table 4; Figure 9) and the linear correlations of turbulent fluxes versus meteorological variables (Table 5). In addition, variations more in LE than H suggest that intraseasonal variations in external forcings had larger impacts on LE than H.

Table 5. Correlation coefficients between LE (H) and meteorological variables on different timescales. For each timescale, the linear relationship was assessed first for the overall year and then separately for the cool season and the warm season. All available data points in 2008 and 2009 were employed. $\Delta T = T_w - T_a$; $\Delta e = e_w - e_a$. The correlation coefficients for LE (H) were not the same on different timescales. Seasonal LE was most associated with Δe, followed by Rn, while was most associated with UΔe for daily and 30-min timescales. H was typically most associated with UΔT on all timescales. LE were more related to H in the cool season.

		LE								H			
		ΔT	**UΔT**	**Δe**	**UΔe**	**U**	**H**	**Rn**	**Res**	**ΔT**	**UΔT**	**U**	**Rn**
Seasonal	**Overall**	0.26	0.22	0.86	0.86	0.20	0.02	0.50	0.02	0.58	0.75	0.00	0.18
	Cool	0.50	0.37	0.84	0.88	0.11	0.27	0.05	-	0.69	0.84	0.02	0.19
	Warm	0.30	0.51	0.64	0.61	0.08	0.20	0.08	-	0.74	0.90	0.00	0.18
Daily	**Overall**	0.45	0.46	0.61	0.83	0.02	0.42	0.11	0.30	0.80	0.92	0.02	0.04
	Cool	0.61	0.65	0.66	0.90	0.08	0.67	0.00	-	0.81	0.93	0.03	0.07
	Warm	0.41	0.48	0.47	0.68	0.02	0.45	0.01	-	0.82	0.94	0.00	0.06
30-min	**Overall**	0.22	0.30	0.45	0.64	0.05	0.27	0.02	0.04	0.66	0.82	0.02	0.04
	Cool	0.44	0.54	0.52	0.79	0.11	0.53	0.00	-	0.68	0.84	0.03	0.04
	Warm	0.07	0.19	0.33	0.47	0.06	0.18	0.02	-	0.62	0.76	0.01	0.05

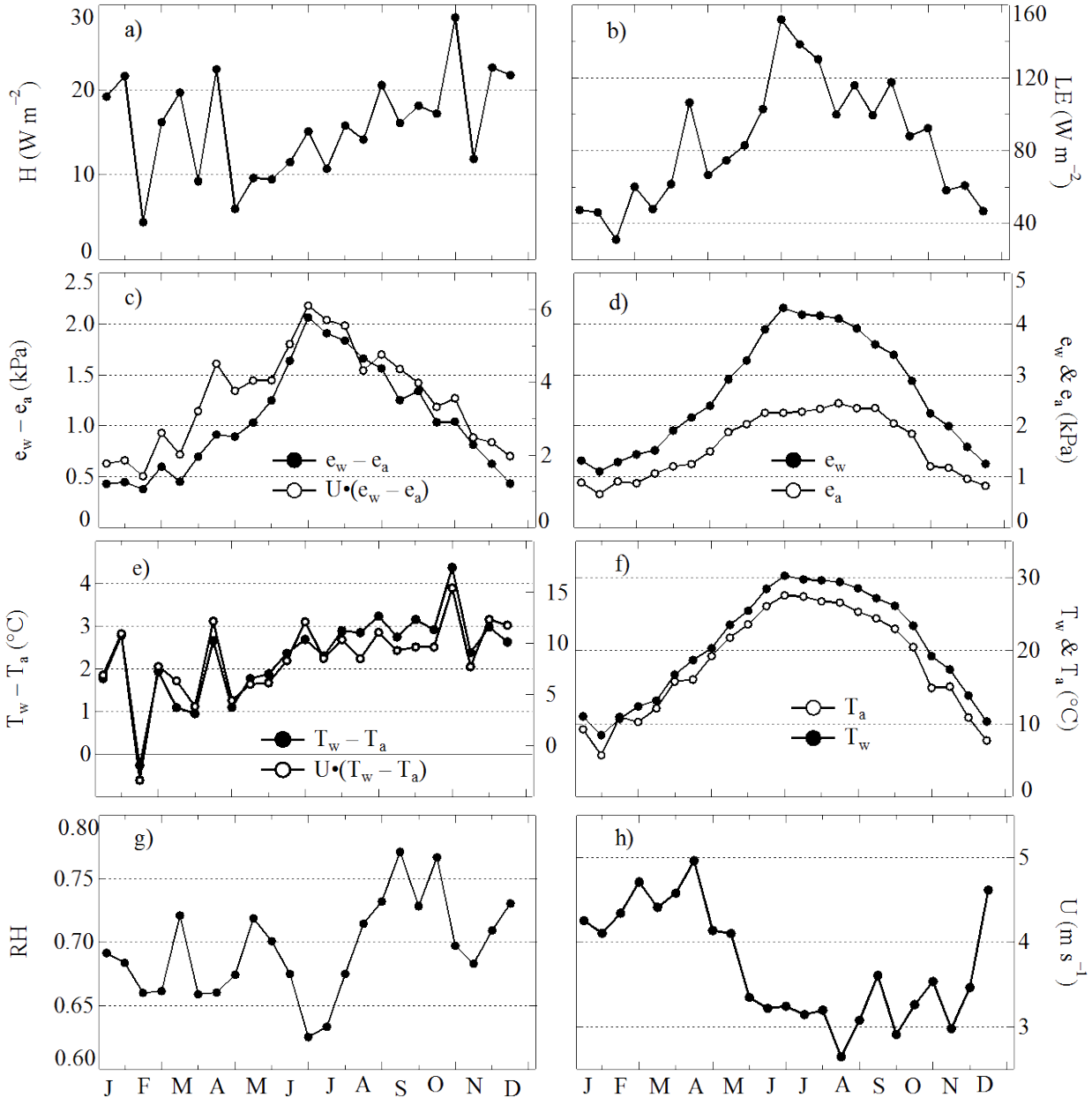

Figure 9. Two-year averaged components of the surface energy budget and meteorological variables (averaged half-monthly means of 2008 and 2009). Quantities include (a) sensible heat flux (H; W m^{-2}), (b) latent heat flux (LE; W m^{-2}), (c) water-air pressure difference ($\Delta e = e_w - e_a$; kPa) and its product with wind speed ($U\Delta e$; kPa m s^{-1}), (d) water vapor pressure (e_w; kPa) calculated from water temperature and air vapor pressure (e_a; kPa), (e) water-air temperature difference ($\Delta T = T_w - T_a$;˚C) and its product with wind speed ($U\Delta T$; ˚C m s^{-1}), (f) water temperature (T_w; ˚C) and air temperature (T_a; ˚C), (g) relative humidity (RH), and (h) wind speed (U; m s^{-1}). Data gaps for the second half of May 2009 and second half of December in both years were due to instrument failures, calibrations, and precipitation

3.3.2 Factors controlling seasonal variations in H

Our results indicate that the seasonal variations in H can be primarily explained by similar patterns in $T_w - T_a$, with a linear correlation coefficient of 0.58 (Table 5; Figures 9a, 9e). The half-monthly averages of both T_a and T_w increased and reached their maximum in late June (27.6˚C for T_a and 30.3˚C for T_w), dropping off afterwards as the months progressed into winter (Table 4; Figure 9f). On a half-monthly basis, T_w was typically larger than T_a throughout the year, creating a positive upward temperature gradient $T_w - T_a$ (Figure 9e). Correspondingly, a thermally unstable, convective ASL developed and, thus H was positive in all months (Figure 9a). $T_w - T_a$ was lowest in early February and March (0 to 1˚C), increased afterwards, reached its maximum in late October (4.4˚C), and then slightly decreased in winter, corresponding well to the half-monthly patterns in H (Figure 9a and 9e; Table 4).

In general, U was small from late May to November (around 3.5 m s^{-1}), and relatively large in the other months (around 4.5 m s^{-1}) (Table 4). The half-monthly means of U showed no correspondence with H, with their correlation coefficients close to zero (Figures 9a, 9h; Table 5). However, multiplying $T_w - T_a$ by U slightly modified its variation pattern, but largely improved the overall linear relationship with H (i.e., R^2(H vs. ΔT) = 0.58, R^2(H vs. $U\Delta T$) = 0.75; Table 5). This indicates that although U was important in controlling the turbulent exchange by inducing

the mechanical mixing, it functioned in a nonlinear way. It is also interesting to note that both the linear correlation coefficients of H with $T_w - T_a$ and $U(T_w - T_a)$ were consistently larger in the warm season (R^2 = 0.74 and 0.90; Table 5) than in the cool season (R^2 = 0.69 and 0.84; Table 5). This implies that relationships between H and $T_w - T_a$ were more robust in the warm season than in the cool season on the seasonal timescale. *In summary, our results indicate that $T_w - T_a$ was the primary factor affecting seasonal variation patterns in H, and including U improved this correlation.*

3.3.3 Factors controlling seasonal variations in LE

Our results showed that seasonal variations in LE were best explained by similar variations in $e_w - e_a$ (R^2 = 0.86; Table 5) followed by Rn (R^2 = 0.50; Table 5). The water-air interface was typically at saturation, and the vapor pressure at this interface was the saturation vapor pressure, which was a function of the surface temperature. Given the fact that the half-monthly average T_w was larger than the T_a in the ASL, the saturation vapor pressure at the water-air interface (quantified by e_w here) was always greater than the saturation vapor pressure in the ASL with T_a. Because it was subject to the influence of air masses from surrounding landscapes, however, the over-water air was not even close to saturation, with its half-monthly average RH ranging from 63% to 77% (Table 4). As a result, e_w was typically larger than e_w (Figure 9d). Temporal

variations in both e_w and e_a led to $e_w - e_a$ increasing as the seasons progressed, reaching its maximum in the summer (2.07 kPa in late June; Table 4) , and decreasing afterwards (Table 4, Figure 9c). Given the sufficient mechanical mixing (as reflected by U in Figure 9h) and the unstably stratified ASL (as reflected by positive $T_w - T_a$), seasonal variations in LE followed those of $e_w - e_a$ fairly well (Figures 9b, 9c). This was also supported by the large correlation coefficient between LE and $e_w - e_a$ ($R^2 = 0.86$; Table 5). However, multiplying $e_w - e_a$ with U resulted in no improvement for the correlation between LE and $U(e_w - e_a)$ ($R^2 = 0.86$, Table 5), even though the correlation between U and LE was weak ($R^2 = 0.20$). This indicates that U influences LE in a nonlinear way. Different from H, the higher linear correlation coefficient between LE and its controlling factors occurred in the cool season rather than in the warm season, suggesting that the linear relationship between LE and the controlling factors is stronger in the cool season.

In summary, the surface energy budget over the water exhibited clear seasonal variations in correspondence to seasonal variations in external forcings, such as $T_w - T_a$, $e_w - e_a$, U, and Rn. To better understand how external forcings control temporal variations in H and LE requires examining how H and LE responded to changes in external forcings diurnally, which is discussed in the next section.

3.4 Diurnal variations

3.4.1 General diurnal variations in the surface energy budget

The general features of diurnal variations in Rn, H, and LE can be analyzed through their two-year monthly averaged diurnal cycles for each month (Figure 10). Rn presented a clear, bell-shaped diurnal cycle for each month, with maximum values (positive) in the early afternoons and minimum values (negative) during the nighttime. For the two years, the daily maximum Rn was largest in June (725.1 W m^{-2}) and smallest in January (231.2 W m^{-2}). On average, the water gained net radiative heating during the daytime and experienced a net loss of longwave radiation at night. As a consequence, the water surface temperature (T_w) exhibited a diurnal variation similar to that of Rn with some phase lags, with its minimum values occurring in the early morning and maximum values occurring in the late afternoon (Figure 11).

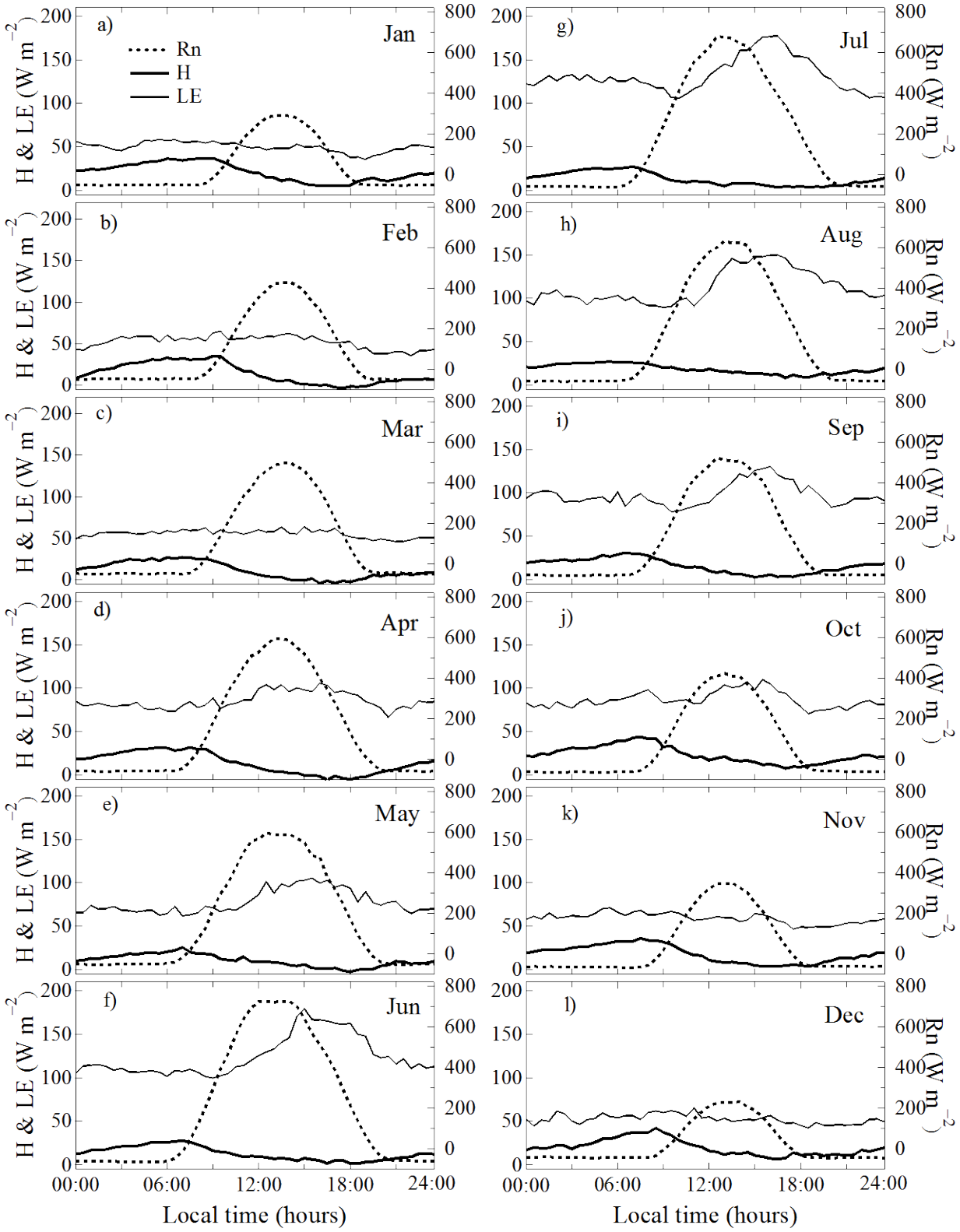

Figure 10. Two-year averaged monthly diurnal cycles of Rn, H, and LE. LT (local time)

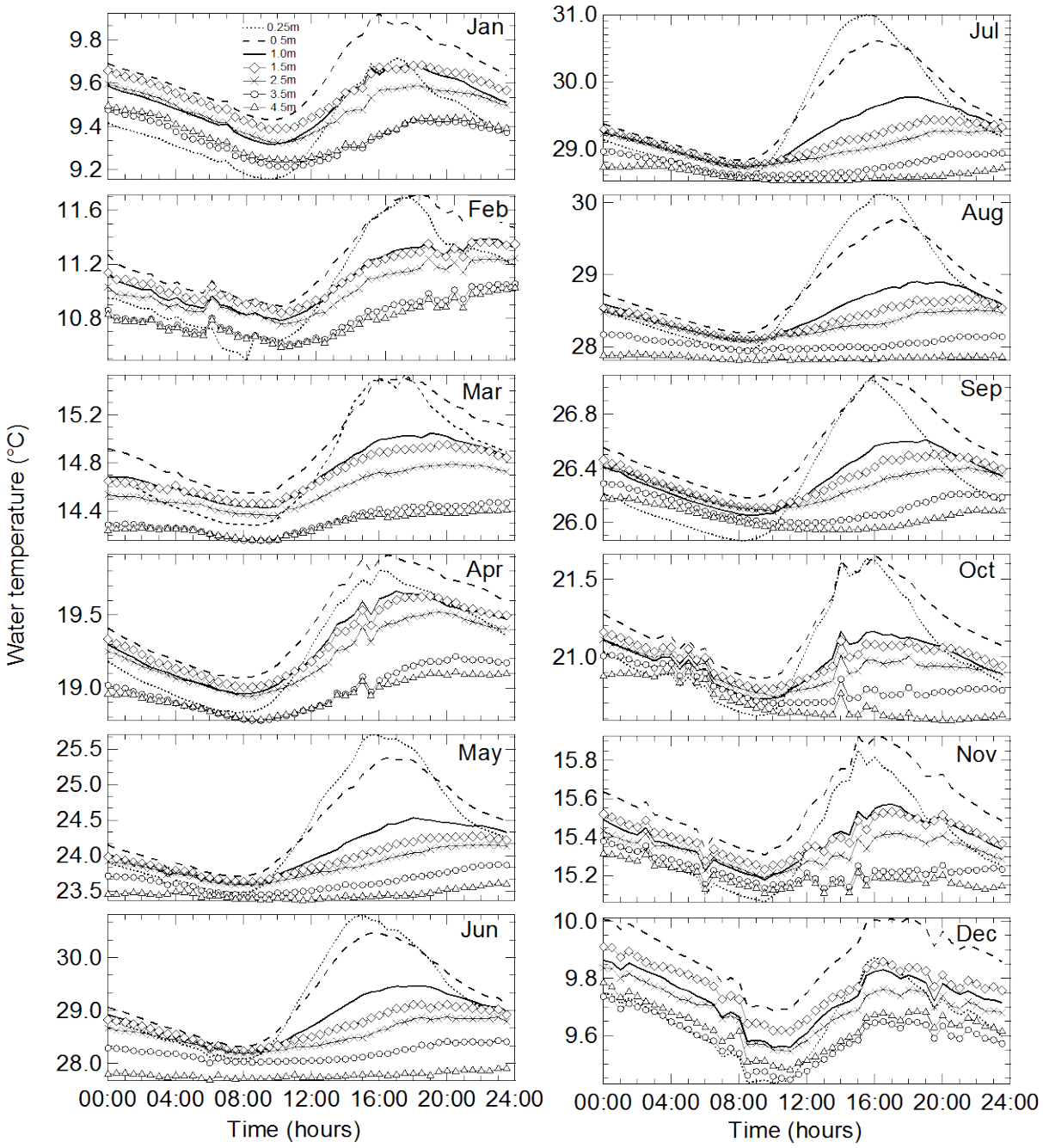

Figure 11. Two-year averaged monthly diurnal cycles of water surface temperatures at different depths

Our data also indicate an exponential decrease in the diurnal wave amplitudes of water temperatures with depths and a progressive phase shift of wave amplitudes with depths (Figure 11). However, the diurnal wave amplitudes were generally small compared to the air. For example, the diurnal wave amplitudes for the water surface temperature were largest in July (5.1°C) and smallest in January (1.4°C). Small diurnal variations in the water temperature at a depth of 4.5 m were still observed, with the largest occurring in February (0.7°C) and the smallest in August (0.1°C). Relatively small wave amplitudes for water temperatures at different depths, as compared with those for soil, were attributed to the direct heating of the water by solar radiation, which penetrated down through the deep layers, as well as significant heat transfer and vertical mixing in the water layers via large eddy diffusion.

It is noted that the monthly average diurnal cycles of H and LE showed no correspondence to those of Rn (Figure 10). Even when Rn was negative during nighttime, H and LE were not zero and contribute substantially to the daily means for each month. This reflected that Rn was not the direct driving force for H and LE on the diurnal timescale. However, the correspondence of large Rn and LE in the summer shows that Rn limited the energy supplied for LE in the long run. On a daily basis, the water temperature increases as the water absorbs and stores energy (Rn), creating a time lag between Rn and LE.

H exhibited diurnal sine waves, with maximums occurring in the early morning and minimums in the late afternoon. The daily maximums for H were largest in October (44.0 W m^{-2}) and smallest in May (25.5 W m^{-2}) for the averaged two years. The monthly average diurnal cycles of LE showed two kinds of patterns (Figure 10). In the cool season (i.e., October to March), the diurnal variations in LE roughly followed those of H. For the warm season (i.e., April to September), the bell-shaped LE developed with its maximums in the late afternoon. The daily maximum LE was largest in June (179.2 W m^{-2}) and smallest in January (58.6 W m^{-2}) (Figure 10). To emphasize the different controlling factors that influence diurnal variations in H and LE in the warm and cool seasons, we selected two periods to represent the winter and summer cases in 2008 for our analysis in the next two sections: January, February, and March (hereafter JFM) and June, July, and August (hereafter JJA).

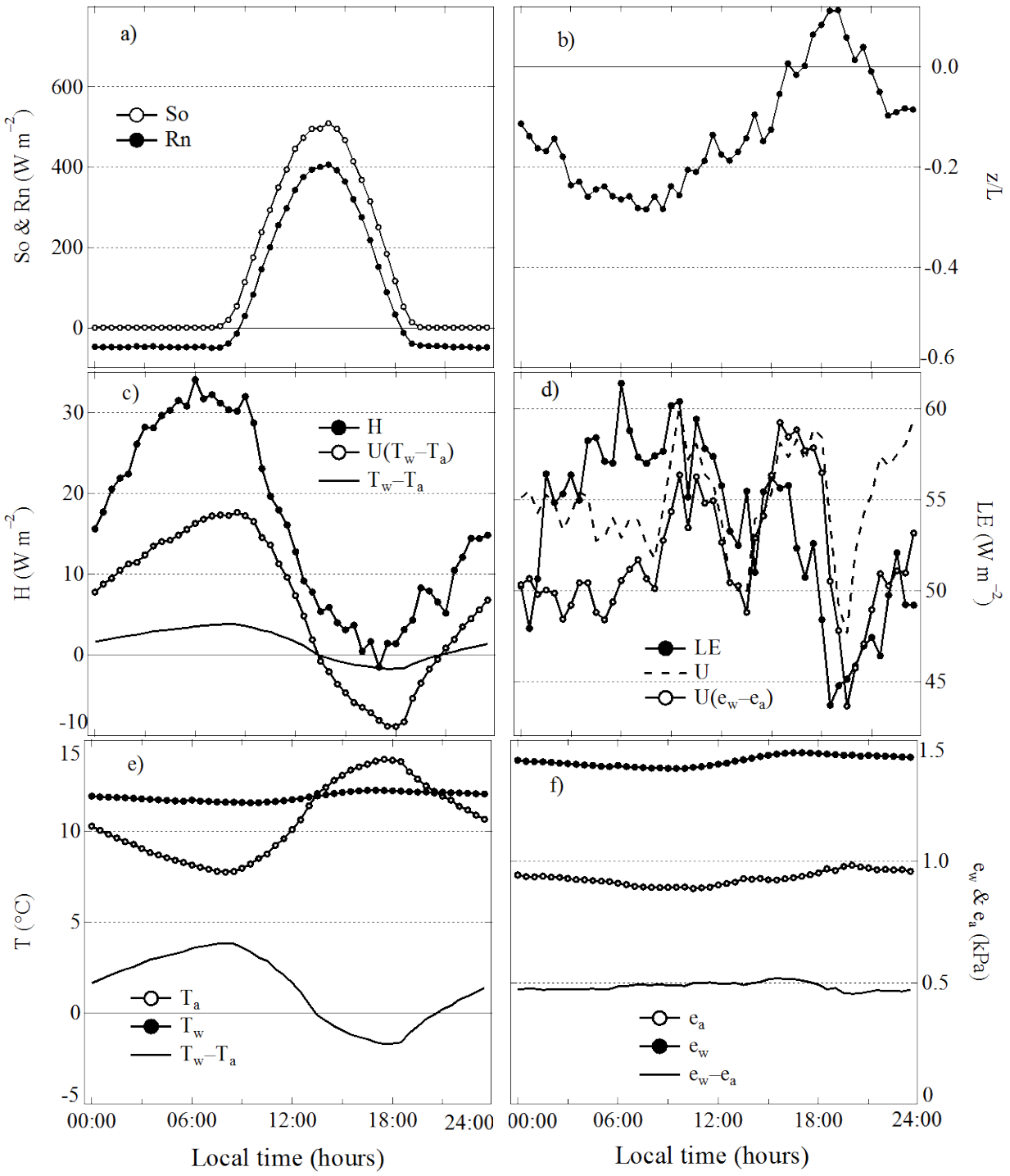

Figure 12. Diurnal variations of energy fluxes and meteorological variables in the 2008 winter (January, February, and March). Note that the right axis only shows scales for LE and other variables were adjusted in their magnitudes to best match the variations in LE. z/L: the stability parameter where z is the measurement height and L is the Monin-Obukhov length).

3.4.2 Diurnal variations and controlling factors in winter (JFM)

In the cool season, as represented by winter, both Rn and S_o were small, with daily maximums of about 400 ~ 500 W m^{-2} (Figure 12a). H presented strong diurnal sine-wave cycles with relatively large amplitudes (about 35 W m^{-2}), reaching daily maximum (34.1 W m^{-2}) at 0600 LT (Local Time) and a minimum (–1.5 W m^{-2}) at 1700 LT.

Our results indicated that these diurnal variation patterns for H were best explained by similar patterns in $T_w - T_a$ (R^2 = 0.94; Figure 13). Though diurnal variations for both T_w and T_a displayed clear sine waves, the amplitudes of T_w was consistently much smaller than those of T_a, leading $T_w - T_a$ to reach its maximum in the early morning (about 0700 – 1000 LT) and minimum in the late afternoon (about 1800 – 2000 LT) (Figure 12e). The daily $T_w - T_a$ was greater than zero for most of the time but became negative for a certain period in the late afternoon or early evening. Consequently, such diurnal variation patterns in $T_w - T_a$ created the ASL stratifications (reflected by the stability parameter z/L where z is the measurement height and L is the Monin-Obukhov length) that were stable for a certain period in the late afternoon and unstable during the rest of the periods (Figure 12b). The strongest unstable stratification (z/L = –0.3) of the ASL occurred in the early morning with the largest $T_w - T_a$ (positive), and the weakest unstable stratification (z/L = –0.1, even turning into a weakly stable stratification with a

z/L of up to 0.1) occurred in the late afternoon with the smallest $T_w - T_a$ (even turning into a negative value). Note that this diurnal variation in stability over water is different from over land [*Stull*, 1988].

The diurnal variations in LE were weak in their magnitudes and roughly followed those of H, with relatively large values in the daytime (about 55 ~ 60 W m^{-2}) and small values during the late afternoon and evening (about 45 W m^{-2}) (Figure 12d). In winter, the over-water air was very dry under the influence of continental air masses, and e_w was also low due to the low water surface temperature. Both e_w and e_a exhibited little diurnal cycles (Figure 12f). As a result, diurnal variations in $e_w - e_a$ were fairly small, with their magnitudes varying around 0.5 kPa. However, the mechanical mixing was remarkably strong during these months, as indicated by the high U (Table 4). Under these conditions, the diurnal variations in LE were likely to be controlled more by the ASL stability than by $e_w - e_a$, leading to the close correspondence between LE and z/L ($R^2 = 0.67$, Figure 13). The linear correlations between LE and U ($R^2 = 0.02$) as well as between LE and U($e_w - e_a$) ($R^2 = 0.10$) were very weak (Figure 13).

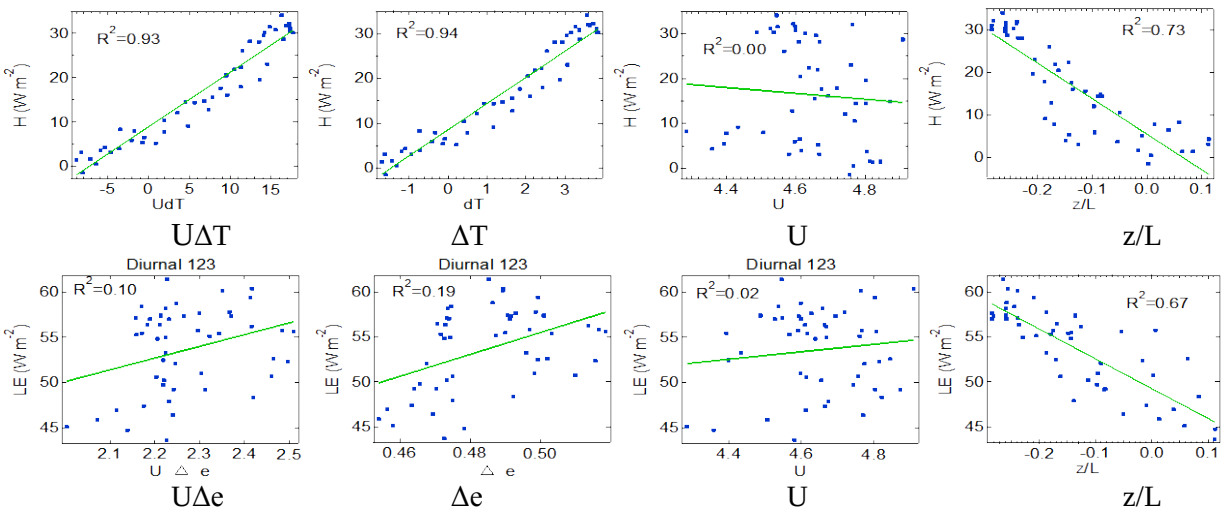

Figure 13. Linear regressions of the diurnal H against UΔT, ΔT, U, and z/L as well as the diurnal LE against UΔe, Δe, U, and z/L in winter

3.4.3 Diurnal variations and controlling factors in summer (JJA)

In summer, both S_o and Rn were large, with daily maximums of around 650 ~ 700 W m^{-2} (Figure 15a), providing large energy inputs to the water. H showed similar diurnal variations as in winter but with smaller amplitudes (about 5 W m^{-2} smaller for the daily maximum and 5 W m^{-2} larger for the daily minimum). The daily $T_w - T_a$ was always greater than zero. Reflected by z/L, the ASL was unstable except for a short period in the late afternoon, in which the ASL was weakly stable (Figure 15b). In addition, the ASL was more unstable in the warm season than in the cool season, as indicated by the magnitudes (Figure 12b vs. Figure 15b). Note again that this diurnal cycle of the ASL stability is completely different from that over land [*Stull*, 1988].

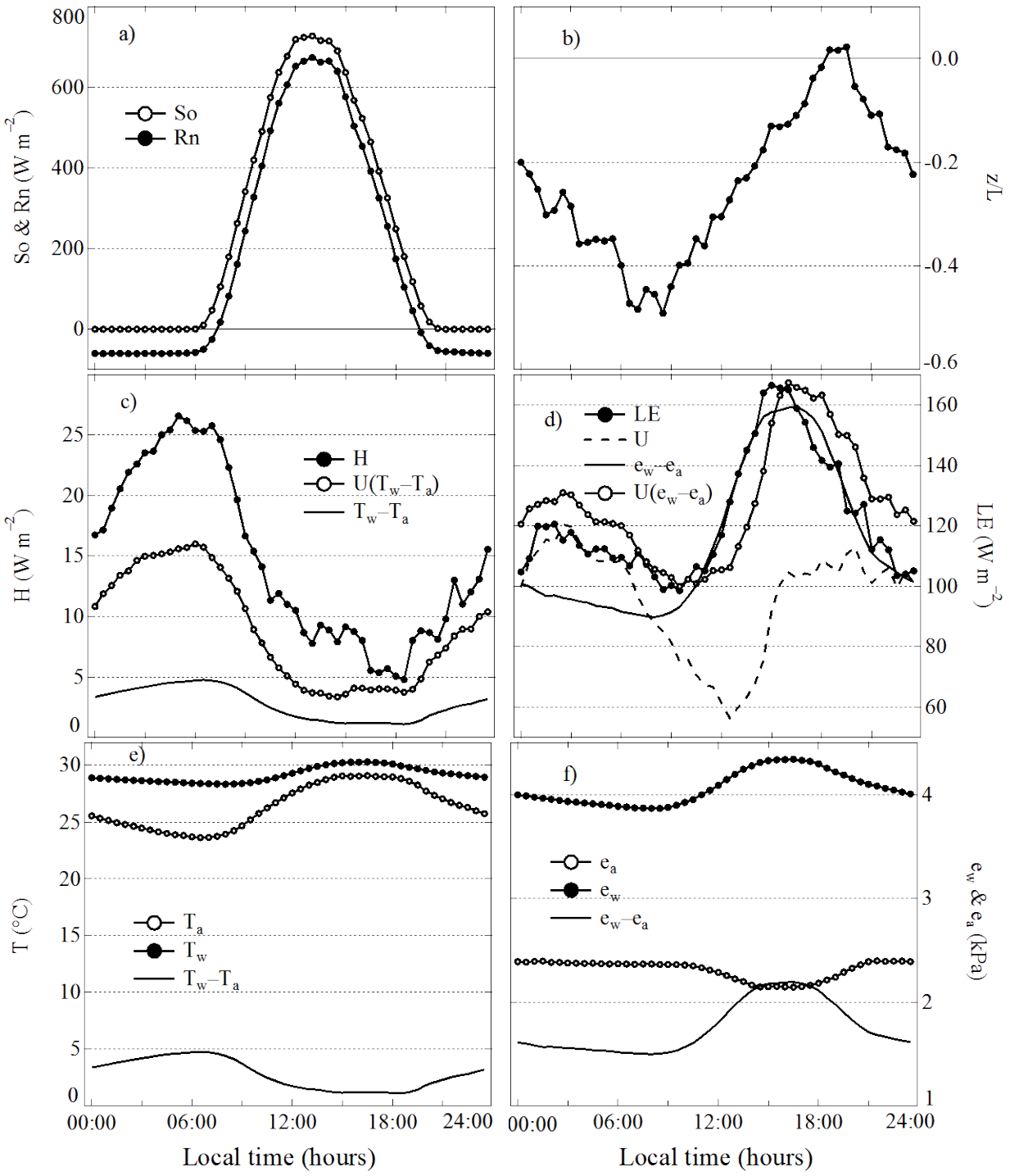

Figure 14. Diurnal variations of the surface energy fluxes and meteorological variables in the 2008 summer (June, July and August). Note that the right axis only shows scales for LE and other variables were adjusted in their magnitudes to best match the variations in LE

Diurnal variations in H were best explained by those in ΔT alone (R^2 = 0.95; Figure 14). Multiplying ΔT with U resulted in a slightly weaker correlation between H and UΔT (R^2 = 0.94; Figure 14). H was still poorly correlated with U (R^2 = 0.11, Figure 14), but better than the relationship in winter (R^2 = 0.00, Figure 13). In addition, H was moderately correlated with z/L (R^2 = 0.58; Figure 14), which was weaker than that in winter (R^2 = 0.73, Figure 13).

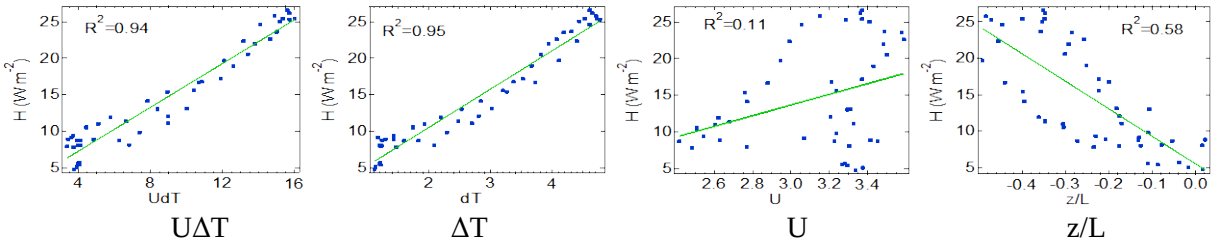

Figure 15. Linear regressions of the diurnal H against UΔT, ΔT, U, and z/L in summer

Diurnal variations in LE presented a bell-shape with its maximums (about 165 W m^{-2}) in the late afternoon (Figure 15d). Both e_w and e_a had larger magnitudes and larger vapor pressure gradients (i.e., $e_w - e_a$ that varied from 1.5 to 2.2 kPa) compared with those in the winter (i.e., $e_w - e_a$ that varied from 0.4 to 0.5 kPa; Figure 15f). Turbulent mixing, represented by wind speeds, was sufficient (2.4 ~ 3.6 m s^{-1}) with minimums at noon (Figure 15d). As a consequence, LE was considerably larger in summer than in winter in terms of its diurnal variation magnitudes. Linear regressions of LE against external forcings on the diurnal basis were applied to interpret the summertime LE diurnal cycle (Figure 16, upper panels). No linear relationship was found between LE and U (R^2 = 0.00; Figure 16a). The linear relationship between LE and U($e_w - e_a$)

was stronger (R^2 = 0.61; Figure 16b). The strongest linear correlation existed between LE and $e_w - e_a$ (R^2 = 0.88; Figure 16c). It is surprising that including U with $e_w - e_a$ (i.e., $U(e_w - e_a)$) did not improve the relationship between LE and $e_w - e_a$. However, further investigations showed that the data points were distributed regularly, instead of randomly, in these linear regression plots, and these data points followed a specific temporal sequence (Figure 16, bottom panels). The LE vs. U plot basically formed a circular sequence (Figure 16d, while the LE vs. $e_w - e_a$ plot was close to a straight line (Figure 16e). The product of U and $e_w - e_a$ led to a LE vs. $U(e_w - e_a)$ pattern which had a unique elliptical, temporal sequence.

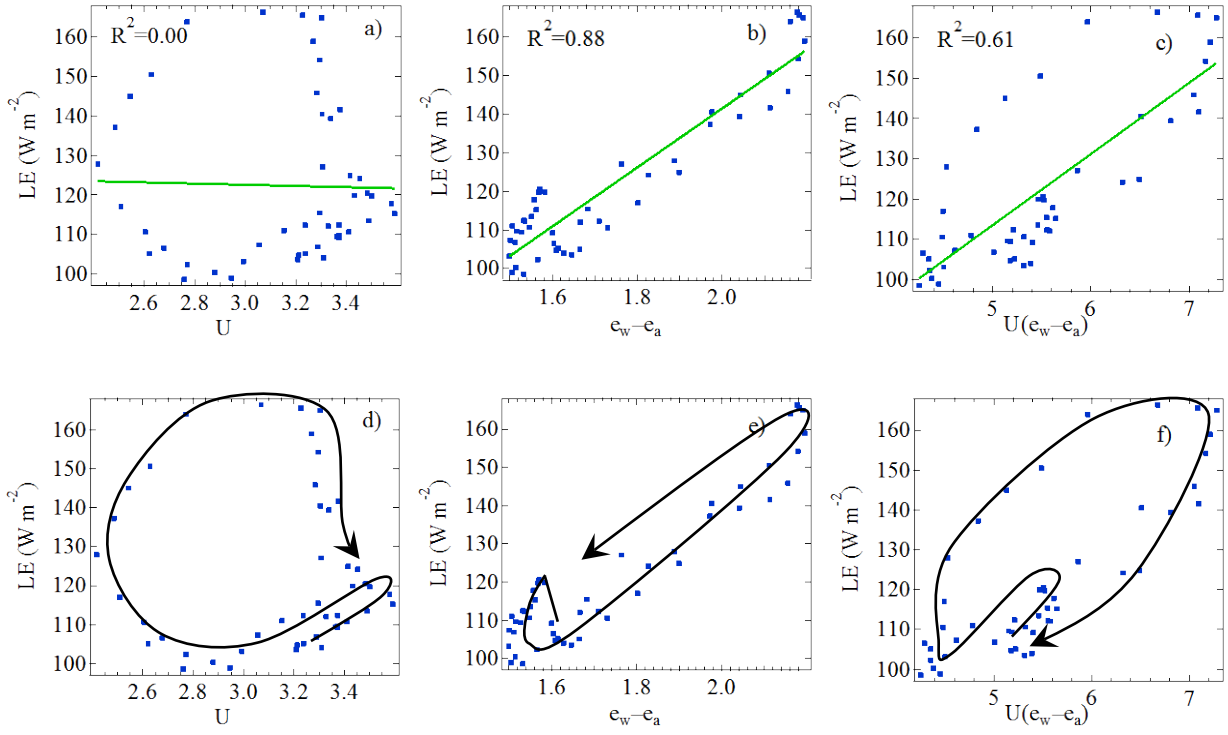

Figure 16. Linear regressions (upper panels) and temporal sequences (lower panels) of LE against U, $e_w - e_a$, and $U(e_w - e_a)$ in the summer. The arrow points toward the end of the day

This elliptical pattern was actually present in the linear regression of LE against $U(e_w - e_a)$ when all summertime 30-min runs were used (Figure 23; Section 3.7), due to the overlaps of many diurnal elliptical patterns on one plot. The sharp change in LE, when $U(e_w - e_a)$ approached zero, was actually the consequence of this elliptical pattern (Figure 23). It is noted from these sequences that LE was not linearly correlated with U and that the direct product of U and $e_w - e_a$ may not result in the best explanation for the diurnal cycles of LE. In addition, it suggests that the nonlinear relationship between LE and external forcings may be overlooked in any linear regression practice; thus one should apply this method with cautions when assessing the turbulent exchange by using Eq. (17) (Section 3.7).

Based on the temporal sequences shown in Figure 16, it is speculated that external forcings such as U, $e_w - e_a$, and $U(e_w - e_a)$ may play relatively important roles in different time intervals to govern the temporal variations in LE. Because U and $e_w - e_a$ did not always vary at the same direction (i.e., increase or decrease), the phase lags between LE and $U(e_w - e_a)$ were generated (Figure 14d). From 0000 LT to 0900 LT, LE closely followed the variations in U since there was little change in $e_w - e_a$. After 0900 LT, $e_w - e_a$ increased substantially and played an increasing role in controlling the change in LE, despite a decrease trend in U (Figure 15d). This means that the mechanical mixing during the period with the weak winds was still strong enough to maintain sufficient turbulent exchange and lead to the large LE, given the presence of the

unstable ASL (Figure 15b). In the late afternoon, the combined effect of the decreased instability (even a stable ASL) and the decreased $e_w - e_a$ led to a decrease in LE, under the circumstance of the unchanged mechanical mixing (i.e., a little change in U) (Figure 15d). *In summary, the diurnal cycle of LE was alternately affected by U and $e_w - e_a$, leading to a phase lag almost always between LE and U($e_w - e_a$).*

3.5 H and LE pulses and their contributions to interannual variations in H and LE

It was seen in Figures 5 and 7 that the intraseasonal variations of H and LE were superimposed with occasionally large H and LE pulses throughout the years. Therefore, analyzing the H and LE pulses (i.e., their intensity, duration, and frequency) and physical processes in producing these pulses should enable us to better understand how these H and LE pulses modulate intraseasonal, seasonal, and interannual variations in the surface energy budget.

3.5.1 Definition of H and LE pulses

In previous studies on high-latitude lakes or southern ones in the cool season [*Blanken et al.*, 2000; *Liu et al.*, 2009], H (LE) pulses were defined as increased sensible (latent) heat flux events when the daily mean H (LE) was at least 1.5 times the value of the centered 10-day running

mean of H (LE). H and LE pulses were also found to be almost coincident to each other. Our results showed that H in summer had small magnitudes (i.e., 14.3 – 14.6 W m^{-2}; Figure 17) and experienced regular variations that could easily exceed its centered 10-day running mean while LE experienced no such variations (Figure 18). Therefore, we adopted a more reasonable definition for a H and LE pulse (hereafter pulse in short) that both H and LE should be at least 1.5 times the value of the respective centered 10-day running mean of H and LE. Based on this definition, we identified a total of 35 and 32 pulses in 2008 and 2009, covering a total of 55 and 53 days, respectively (Figures 17, 18). In addition, based on the observations from synoptic weather charts (chart sources: http://www.hpc.ncep.noaa.gov/dailywxmap/), there were three and four cold fronts that passed over the study site during the data gap period in the cool season of 2008 and in the warm season of 2009, respectively. Therefore, it is reasonable to assume that three and four pulses were probably produced during these periods. These pulses need to be taken into account to limit errors to the minimum levels. To account for the duration of these pulses, we assumed that each pulse lasted for one day such that the total pulse days were added up to 58 and 57 days in 2008 and 2009, respectively. To account for the magnitude of these pulses, we filled the pulse gap days with the daily averages obtained from all available pulses in each season. The other days excluding pulses during the data gap period were considered as non-pulse days and were filled with the daily averages of all available non-pulse days in each season. Data gaps in the meteorological variables were also filled using the same procedure.

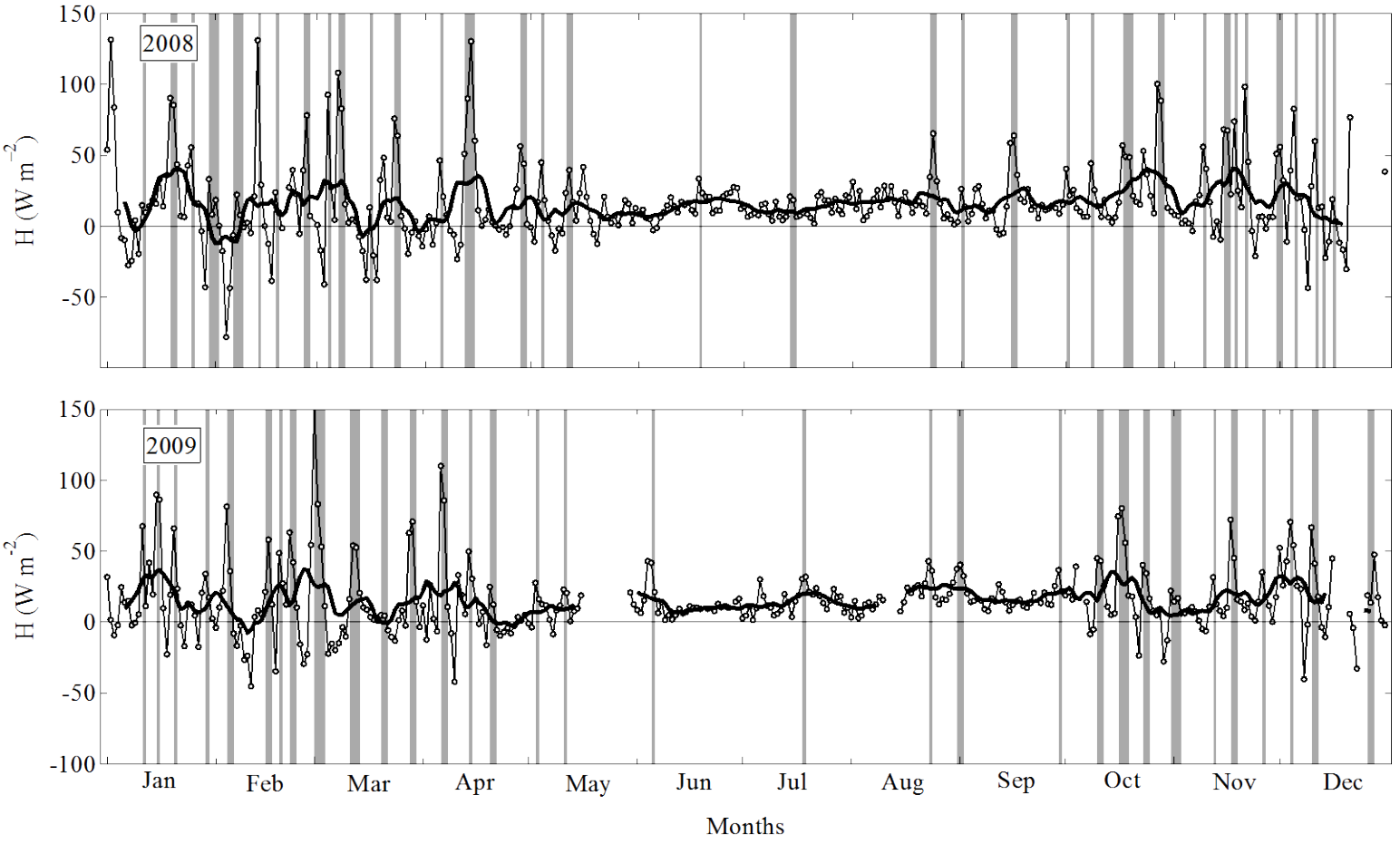

Figure 17. Daily means (lines with circles) and the centered 10-day running mean (bold lines) of H. H pulses were marked as shadows

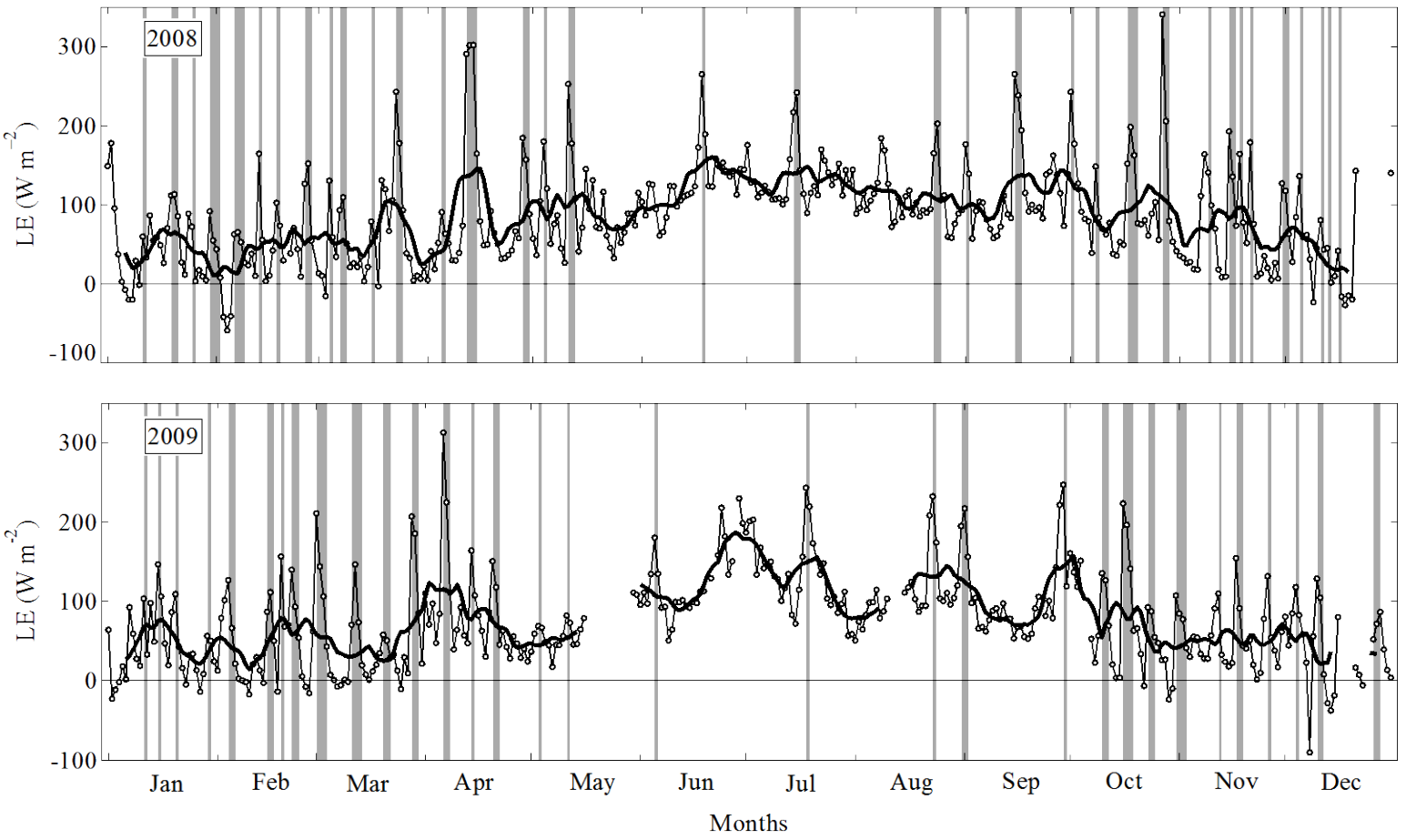

Figure 18. Daily means (lines with circles) and the centered 10-day running means (bold lines) of LE. LE pulses were marked as shadows

3.5.2 Physical processes to generate H and LE pulses

The frequent H and LE pulses were caused by air mass movements that were often associated with cold fronts [*Blanken et al.*, 2000; *Liu et al.*, 2009]. To illustrate how these cold fronts and dry air masses affect H and LE, we examined a pulse that occurred in late February of 2009. The dates on which the cold front was passing over this region was determined by comparing daily synoptic weather charts from consecutive days [*Liu et al.*, 2011]; while the arrival time of the cold front was estimated by examining the time-series data of 30-min mean meteorological variables and H and LE fluxes [*Liu et al.*, 2011].

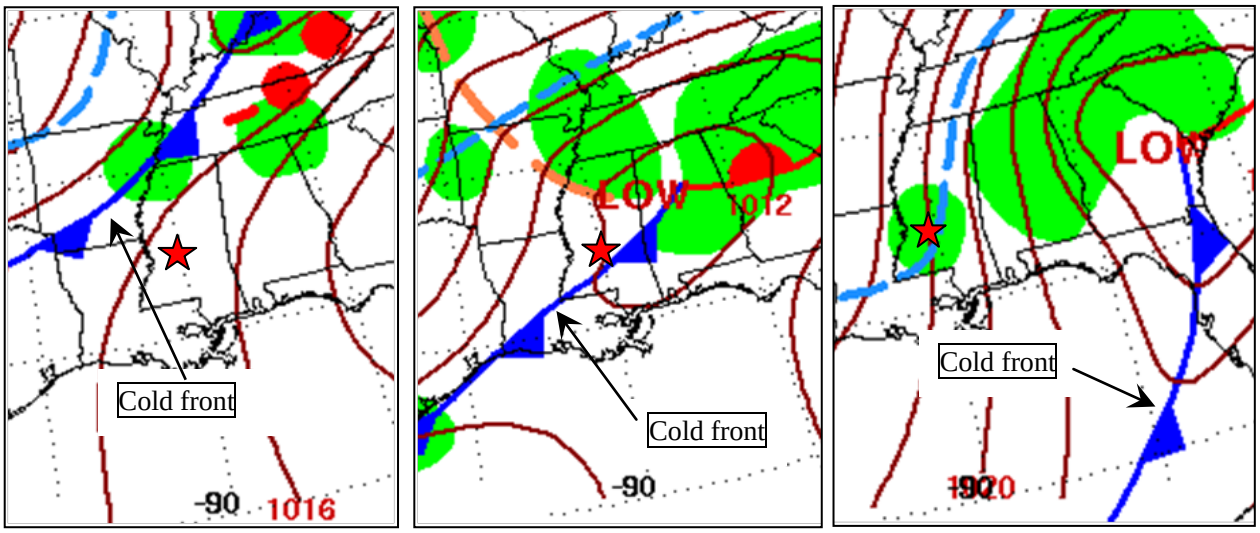

February 27
0600 LT

February 28
0600 LT

March 1
0600 LT

Figure 19. Daily weather maps showing the passage of a cold front in February of 2009 (local time). Star denotes the location of the study site (Chart Source: http://www.hpc.ncep.noaa.gov/dailywxmap/)

The synoptic charts clearly showed that this cold front passed over the site on 28 February 2009 (Figure 19). The time-series data indicated that the cold front arrived at the site at approximately 0300 LT on that day, leading to a high-wind event with a rapid increase in wind speed, a dramatic decrease in temperature, and a large drop in water vapor pressure. After the cold front passage, the site was under the influences of cold and dry air masses for about five days until March 4 (see more discussion below).

Before the cold front, this site was dominated by southerly winds with a mean wind speed of 5.09 m s^{-1} (Table 6; Figures 20, 21). These air masses were warm and humid (T_a = 16.6°C, RH = 0.71, e_w = 1.34 kPa), passing over the relatively cooler water surface (T_w = 12.1°C), leading to a negative $T_w - T_a$ (–4.5°C) and small $e_w - e_a$ (0.07 kPa) (Table 6; Figure 21). Consequently, H was small and even negative in the afternoons and evenings (–20.8 W m^{-2}). LE was also suppressed and close to zero for most of the time (–2.6 W m^{-2}) (Figure 21; Table 6).

Table 6. Comparisons of the energy fluxes and meteorological variables within and outside a pulse event in February 2009. The dates for outside of the pulse event were averaged over 3 days before and 3 days after the event. The duration for the event was averaged over 5 days.

	So	**Rn**	**LE**	**H**	**U**	**T_a**	**T_w**	**ΔT**	**RH**	**e_a**	**e_w**	**Δe**
	W m^{-2}	W m^{-2}	W m^{-2}	W m^{-2}	m s^{-1}	°C	°C	°C		kPa	kPa	kPa
Outside	138.2	104.8	–2.6	–20.8	5.09	16.6	12.1	–4.5	0.71	1.34	1.41	0.07
Within	171.2	85.2	116.9	71.1	5.56	5.6	11.7	6.1	0.61	0.58	1.38	0.80
Difference	33.0	–19.6	119.5	91.9	0.47	–11.0	–0.4	10.6	–0.10	–0.76	–0.03	0.73

After the cold front's passage, wind directions shifted immediately from the south to the north, with an increase in wind speeds from 5 m s^{-1} to 11 m s^{-1} and then a decrease steadily towards the pulse end (Table 6; Figures 20, 21). Meanwhile, T_a decreased by 11°C while e_a decreased by 0.76 kPa after the passage of the cold front (Table 6; Figure 21). Due to the large heat capacity of water, T_w only decreased by 0.4°C and e_w decreased by 0.03 kPa. As a result, large gradients of temperature ($T_w - T_a$) and vapor pressure ($e_w - e_a$) between the water surface and the overlying air were produced ($T_w - T_a$ = 6.1°C, $e_w - e_a$ = 0.80 kPa). Resulting from the combined effect of the enhanced mechanical mixing, increased vertical gradients ($T_w - T_a$, $e_w - e_a$), and enhanced instability (as reflected by $T_w - T_a$), H and LE were significantly promoted during the pulse days (i.e., H increased by 71.1 W m^{-2}; LE increased by 116.9 W m^{-2}) (Table 6; Figure 21). Note that the increase in Rn was a result of the cloudless days associated with the high pressure system after the cold front passage (Figure 21).

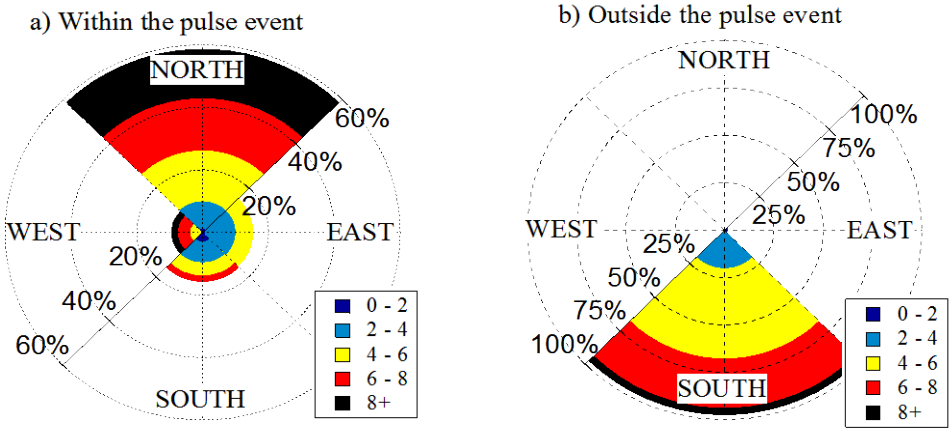

Figure 20. Comparisons of wind directions and wind speeds within and outside a H and LE pulse event in February of 2009

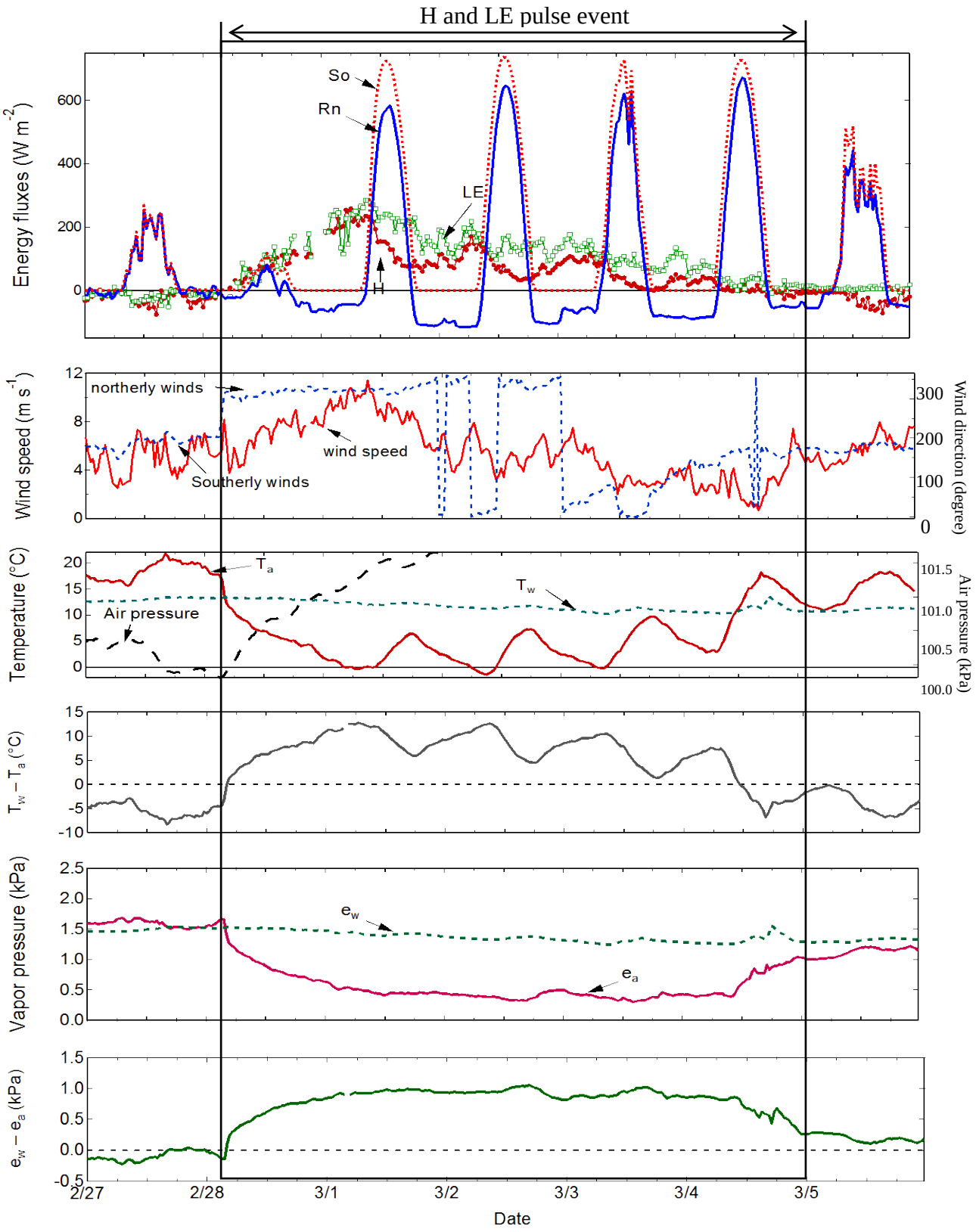

Figure 21. Changes in surface energy fluxes and meteorological variables after a cold front in February 2009

3.5.3 Contributions of H and LE pulses to the surface energy budget

In general, there were 36 ~ 38 pulses per year, covering 57 ~ 58 days (16% of 365 days; Table 7). It was evident that pulses occurred more often in the cool season, covering 22% of the days, than in the warm season, covering 9% of the total days.

To estimate the contribution of H and LE in pulse days to the overall H and LE, both the duration and intensity of the pulses were taken into account using Eq. (16)

$$Ctrn.Flux(PS)\% = \frac{Flux(PS) \times Days(PS)}{Total(Flux)} \times 100\% \quad (16)$$

where Ctrn.Flux(PS)% is the contribution of the flux in percentage to the overall flux, Flux(PS) is the averaged daily mean of the flux during the pulse days, Days(PS) is the pulse days with H and LE pulses. These similar processes were also applied to estimate the contribution of H and LE from the non-pulse days (i.e., Ctrn.Flux(NPS)) to the overall flux. Thus, Flux(NPS) and Days(NPS) denote the daily mean flux and the non-pulse days in each season.

When averaged over the two years, we estimated that H(PS) contributed to 50% of the annual H, reflecting their significant contributions to the overall H (Table 7). On the annual basis, H(PS) was much larger (50.9 W m^{-2}) than H(NPS) (9.4 W m^{-2}), with the annual mean H_m of 15.9 W

m^{-2} (hereafter the subscript m denotes the mean of the quantity under consideration for the discussed period). In the warm season, H(PS) had small magnitudes (46.6 W m^{-2}) and contributed to less than half (30%) of the $H_{m\text{-}warm}$, indicating that $H_{m\text{-}warm}$ was more controlled by H(NPS). In the cool season, H(PS) had large magnitudes (52.7 W m^{-2}) and contributed to more than half (68%) of the $H_{m\text{-}cool}$, indicating that $H_{m\text{-}cool}$ was more controlled by H(PS). Moreover, the smaller H(NPS) in the cool season (7.1 W m^{-2}) than in the warm season (11.4 W m^{-2}) indicates that H and LE pulses enhanced more turbulent exchanges in the cool season in spite of the smaller baseline, leading to larger $H_{m\text{-}cool}$ (17.2 W m^{-2}) than $H_{m\text{-}warm}$ (14.6 W m^{-2}) (Table 7).

Table 7. Two-year averaged daily mean H and LE during the periods of non-pulse days (NPS) and the periods of pulse days (PS) in the cool season, warm season, and the entire year; Ctrn. denotes contribution

		Cool season			Warm season			Annual		
Variable	**Units**	**Overall**	**NPS**	**PS**	**Overall**	**NPS**	**PS**	**Overall**	**NPS**	**PS**
Days	Days	182	141.5	40.5	183	166	17	365	307.5	57.5
Ctrn. Days		100%	78%	22%	100%	91%	9%	100%	84%	16%
H	W m^{-2}	17.2	7.1	52.7	14.6	11.4	46.6	15.9	9.4	50.9
Ctrn. H		100%	32%	68%	100%	70%	30%	100%	50%	50%
LE	W m^{-2}	57.0	38.0	123.5	108.6	98.9	202.9	82.9	70.9	146.9
Ctrn. LE		100%	52%	48%	100%	83%	17%	100%	72%	28%

Averaged over the two years, LE(PS) contributed to 28% of the annual LE, reflecting their substantial contributions to the overall LE (Table 7). On the annual basis, LE(PS) (146.9 W m^{-2}) was about twice LE(NPS) (70.9 W m^{-2}), with the annual mean LE_m of 82.9 W m^{-2}. In the cool

season, LE(PS) contributed to about half (48%) of $LE_{m\text{-}cool}$, and LE(PS) was at least three times LE(NPS), indicating that $LE_{m\text{-}cool}$ was more controlled by LE(PS). All the LE(PS), LE(NPS), and $LE_{m\text{-}warm}$ in the warm season were larger than those in the cool season, indicating the significant contribution of warm-season LE to the overall LE. LE(PS) contributed to a small portion (17%) of the overall $LE_{m\text{-}warm}$ in the warm season (Table 7), indicating $LE_{m\text{-}warm}$ was more controlled by LE(NPS).

3.6 Interannual variations

The overall Rn was slightly larger in 2008 (109.4 W m^{-2}) than in 2009 (106.1 W m^{-2}) (Table 8). Both H and LE were about 10% larger in 2008 (H_m = 16.6 W m^{-2}, LE_m = 86.8 W m^{-2}) than those in 2009 (H_m = 15.2 W m^{-2}, LE_m = 78.9 W m^{-2}). Then what caused these large interannual variations in H and LE despite the small differences in available energy (Rn) and no changes in T_w? *We hypothesize that seasonal variability in high-wind events and the meteorological properties associated with the H and LE pulses modulated heat and water vapor transfer, leading to larger H_m and LE_m in 2008 compared to those in 2009.*

Table 8. Daily means of the energy fluxes and meteorological variables during overall days, non-pulse days (NPS), and pulse days (PS) for the cool and warm seasons as well as for the whole year in 2008 and 2009

			Cool season			Warm season			Annual		
Variable	**Unit**	**Year**	**Overall**	**NPS**	**PS**	**Overall**	**NPS**	**PS**	**Overall**	**NPS**	**PS**
Pulse	Days	2008	182	141	41	183	166	17	365	307	58
		2009	182	142	40	183	166	17	365	308	57
Rn	W m^{-2}	2008	62.2	66.3	47.9	156.4	159.3	128.4	109.4	116.6	71.5
		2009	55.2	55.1	55.7	156.6	158.7	136.6	106.1	110.9	79.8
H	W m^{-2}	2008	18.7	7.9	55.7	14.6	11.0	49.9	16.6	9.6	54.0
		2009	15.7	6.2	49.6	14.6	11.7	43.3	15.2	9.2	47.7
LE	W m^{-2}	2008	63.2	43.9	129.6	110.3	99.2	218.3	86.8	73.8	155.6
		2009	50.8	32.1	117.3	106.9	98.6	187.5	78.9	67.9	138.2
U	m s^{-1}	2008	4.12	3.80	5.20	3.55	3.40	5.00	3.83	3.58	5.14
		2009	3.90	3.70	4.60	3.42	3.30	4.60	3.66	3.48	4.60
$\mathbf{T_a}$	˚C	2008	11.9	13.0	8.0	23.8	24.3	19.4	17.9	19.1	11.3
		2009	12.2	13.2	8.5	24.1	24.7	18.1	18.1	19.4	11.4
$\mathbf{T_w}$	˚C	2008	14.3	14.4	13.9	26.3	26.5	24.7	20.3	20.9	17.1
		2009	14.1	14.0	14.4	26.6	26.9	23.4	20.3	21.0	17.1
$\mathbf{e_a}$	kPa	2008	1.04	1.13	0.71	2.05	2.11	1.49	1.55	1.66	0.94
		2009	1.08	1.17	0.74	2.10	2.17	1.38	1.59	1.71	0.93
$\mathbf{e_w}$	kPa	2008	1.70	1.71	1.67	3.50	3.53	3.17	2.60	2.69	2.11
		2009	1.66	1.65	1.68	3.57	3.63	2.97	2.62	2.72	2.06
$\mathbf{T_w–T_a}$	˚C	2008	2.3	1.2	6.0	2.5	2.2	5.3	2.4	1.7	5.8
		2009	1.9	0.8	5.9	2.6	2.3	5.3	2.3	1.6	5.7
$\mathbf{e_w–e_a}$	kPa	2008	0.66	0.57	0.96	1.44	1.41	1.68	1.05	1.02	1.17
		2009	0.58	0.48	0.94	1.48	1.47	1.60	1.03	1.01	1.14

3.6.1 Factors modulating interannual variations in H and LE

In general, the overall means of T_a for both the cool and warm seasons of 2008 were lower than those in 2009, leading to slightly lower annual mean T_a (17.9°C) which was 0.2°C lower in 2008 than that in 2009 (Table 8). In correspondence to Rn, T_w was higher in the cool season but lower in the warm season in 2008 than that in 2009, leading to a similar annual mean T_w (20.3°C). The air was cooler in 2008 than in 2009; while the water had the same temperature in both years, leading to larger $T_w - T_a$ in 2008 (2.4°C) than 2009 (2.3°C) (Table 8). Consistent with T_w, e_w was very close for the two years, while e_a was lower in all seasons of 2008 (i.e., the annual mean e_a = 1.55 kPa) than those of 2009 (i.e. the annual mean e_a = 1.59 kPa), leading to a slightly larger $e_w - e_a$ in 2008. *In summary, the air was cooler and drier in all seasons of 2008 than 2009, while the water experienced similar annual means in both years, leading to a slightly larger $T_w - T_a$ and $e_w - e_a$ in 2008, as compared with 2009. Nevertheless, $T_w - T_a$ and $e_w - e_a$ were smaller in the warm season of 2008 than in 2009.*

In the warm seasons, Rn and H were fairly close in 2008 (Rn = 156.4 W m^{-2}, H = 14.6 W m^{-2}) to those in 2009 (Rn = 156.6 W m^{-2}, H = 14.6 W m^{-2}) and there was small difference in LE (110.3 W m^{-2} in 2008 vs. 106.9 W m^{-2} in 2009) (Table 8). Thus the major interannual variations must originate from the cool season. It was shown that the overall Rn, H, and LE in the cool season of 2008 (Rn = 62.2 W m^{-2}, H = 18.7 W m^{-2}, LE = 63.2 W m^{-2}) were 13%, 19%, and 24% larger

than those in the cool season of 2009 (Rn = 55.2 W m^{-2}, H = 15.7 W m^{-2}, LE = 50.8 W m^{-2}) (Table 8). Further investigations showed that both non-pulse days and pulse days in the cool season experienced large interannual variations.

During the non-pulse days in the cool season, Rn(NPS) was 20% larger in 2008 (66.3 W m^{-2}) than in 2009 (55.1 W m^{-2}), indicating more available energy for the cool season of 2008 than in 2009 (Table 8). This additional energy explained part of the variations in LE(NPS), which was 37% larger in the cool season of 2008 (43.9 W m^{-2}) than the cool season of 2009 (32.1 W m^{-2}). H(NPS) was 27% larger in the cool season of 2008 (7.9 W m^{-2}) than the cool season of 2009 (6.2 W m^{-2}). Since H and LE during the non-pulse days were more correlated with $T_w - T_a$ and $e_w - e_a$, respectively (Section 3.4), the magnitudes of H(NPS) and LE(NPS) were indicators of the over-water meteorological conditions. Therefore, we expect larger $T_w - T_a$ and $e_w - e_a$ in the cool season of 2008 than in 2009. In fact, our calculations indicated that the mean $T_w - T_a$ and $e_w - e_a$ were 1.2°C and 0.57 kPa, respectively, during the non-pulse days in the cool season of 2008 and 0.8°C and 0.48 kPa, respectively, during the non-pulse days in the cool season of 2009 (Table 8). In addition, the higher T_w in the cool season of 2008 (14.4°C) than in 2009 (14.0°C) indicates that more heat was stored in water to provide primary energy source for H and LE in both non-pulse days and pulse days.

During the pulse days, Rn(PS) was actually smaller in the cool season of 2008 (47.9 W m^{-2}) than the cool season of 2009 (55.7 W m^{-2}) (Table 8). However, both H(PS) and LE(PS) were larger in the cool season of 2008 (H(PS) = 55.7 W m^{-2} , LE(PS) = 129.6 W m^{-2}) than the cool season of 2009 (H(PS) = 49.6 W m^{-2} , LE(PS) = 117.3 W m^{-2}). It was known that H and LE were associated with the intensity, duration, and frequency of high-wind events [*Liu et al.*, 2011]. Given that 2008 and 2009 had similar numbers of H and LE pulses, we expected the larger H(PS) and LE(PS) would imply that the high-wind events were stronger in the cool season of 2008. Our results showed that during the pulse days, U was 13% larger in the cool season of 2008 (5.2 m s^{-1}) than the cool season of 2009 (4.6 m s^{-1}). The slightly larger $T_w - T_a$ and $e_w - e_a$ were also presented during the pulse days of the cool season of 2008. The combination of these factors promoted H and LE exchange during the pulse events more in the cool season of 2008 than in the cool season of 2009. These exchange extracted more energy stored in the water, as reflected by the lower T_w during the non-pulse days in the warm season of 2008 (26.5°C) than in 2009 (26.9°C).

Moreover, it was shown that pulses significantly contributed to the total interannual variations in H and LE fluxes between 2008 and 2009. For H, 80% of its interannual variations were attributed to the interannual variation in pulses, while the remainder 20% was from those in non-pulse days. For LE, 40% of its interannual variations were attributed to those in pulses,

while the remainder 60% was from non-pulse days. *In summary, the interannual variations in the surface energy budget between 2008 and 2009 was mainly caused by the variations in the cool season, in which 2008 had more available energy during the non-pulse days and experienced stronger high-wind events during the pulse days.*

These results suggest that the interannual variations in water surface energy fluxes are strongly dependent upon their variations in cool seasons, due to significant modulation by H and LE pulses. These H and LE pulses are largely determined by the intensity, frequency, and duration of high-wind events associated with synoptic weather conditions. Several studies have shown that cyclone activities have changed in the past decades due to climate change [*McCabe et al.*, 2001; *Teng et al.*, 2008]. Future changes in the intensity, frequency, and duration of cold front activities and the associated high-wind events due to climate change would likely modify the water surface energy fluxes in the cool season and thus alter their annual and interannual variations. It is interesting to know whether climate change will intensify or weaken the water surface energy fluxes because both the meteorological properties associated with high-wind events during H and LE pulse days and the weather conditions during non-pulse days have significant influences on the overall changes. Future studies should pay attention to these questions since evaporative loss of fresh water from inland water bodies, a component of the surface energy budget, could have significant implication for water resource managements through the process of evaporation.

3.6.2 General statistical analysis of winds for 2008 and 2009

Wind rose diagrams enable us to study influences of wind speeds and directions affecting the surface energy exchange (Figure 22; Table 9). The radius of the rose plot is the percentage that winds with certain speeds are within a given direction range. The different colors indicate the wind speed ranges as explained in the legend. In this study, an increment of 90 degree in wind directions and an increment of 2 m s^{-1} in wind speed were used. All winds were categorized into west, north, east, and south.

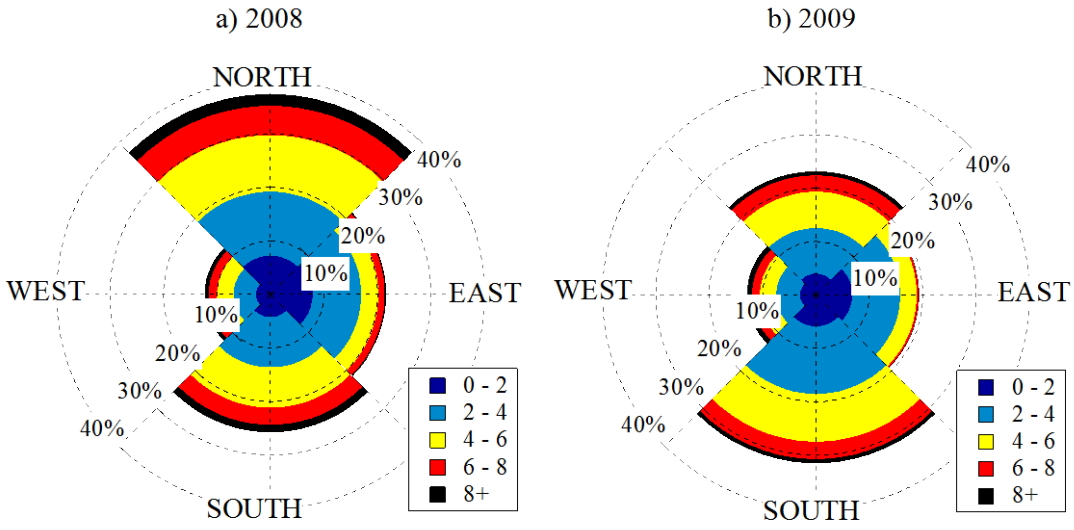

Figure 22. Wind rose diagrams for 2008 and 2009. The radius of the rose plot is the percentage that a wind speed value is within the given direction range. The different colors indicate the wind speed ranges as explained in the legend. In this study, an increment of 90 degree in wind directions and an increment of 2 m s^{-1} in wind speed were used

In the cool season of 2008, the northerly winds were predominant and comprised up to 37% of the annual statistics. It was also apparent that there were more high-wind events in 2008, as reflected by more than 20% of winds at speeds higher than 6 m s^{-1}. In contrast, the southerly winds were predominant in 2009, consisting of 32% of the annual statistics, with a large percentage of speeds between 2 to 6 m s^{-1} (Figure 22; Table 9). In 2009, the northerly winds accounted only for 23% of the annual statistics, with 15% of which at speeds higher than 6 m s^{-1}.

It is speculated that the winds blowing from different directions were affected by various synoptic weather systems such as anticyclones and cyclones, bringing in air masses with different meteorological properties to this region. These different air masses provide distinctive atmospheric forcings and temporal variations on synoptic scales, affecting exchange processes of H and LE over the water surface.

In general, winds from the continent (i.e., west, north, and east) brought in cool/dry air masses, which enhanced temperature and humidity gradients (i.e., $T_w - T_a$, $e_w - e_a$), while southerly winds brought in warm/humid air masses, which reduced the gradients. For example, it is shown in Table 9 that southerly winds were generally associated with lower $T_w - T_a$ and $e_w - e_a$ than the winds from other directions. As a consequence, H and LE were generally promoted under the influence of continental winds, while suppressed under the influence of southerly winds (i.e.,

smaller H and LE for southerly winds in both years, Table 9). Specifically in winter, continental winds promoted LE due to the enhanced mechanical mixing (i.e., higher wind speeds). Therefore, interannual variations in wind directions and wind speeds are likely to contribute partly to interannual variations in H and LE in this region, as more continental winds with higher wind speeds resulted in larger $T_w - T_a$ and $e_w - e_a$, hence larger H and LE in 2008 than in 2009.

Table 9. The 30-min means of components of the surface energy budget and meteorological variables from the west (W), north (N), east (E), and south (S) in 2008 and 2009

	WD		**U**		**H**		**LE**		**$e_w - e_a$**		**$T_w - T_a$**	
	%		$m\ s^{-1}$		$W\ m^{-2}$		$W\ m^{-2}$		kPa		°C	
	2008	2009	2008	2009	2008	2009	2008	2009	2008	2009	2008	2009
W	13%	13%	3.98	3.96	17.9	17.2	114.5	110.2	1.25	1.18	2.4	2.3
N	37%	23%	4.05	4.20	26.4	35.0	99.6	123.3	1.00	1.14	3.0	4.1
E	22%	19%	2.93	2.77	14.9	16.5	86.7	75.0	1.22	1.10	2.8	3.0
S	25%	32%	4.12	3.77	6.4	1.8	67.8	44.1	1.06	0.79	1.6	0.4

3.7 Mechanisms controlling turbulent exchanges

It is well known that LE over water surface depend largely on the vertical gradient of vapor pressure at the water-air interface (i.e., $e_w - e_a$) as well as on intensity of turbulent mixing [*Bonan*, 1995; *Hendersonsellers*, 1986; *Hostetler and Bartlein*, 1990]. In numerical models, the mass transfer method (Eqs. (17), (18)) was used extensively for estimating the LE over lakes and reservoirs [*Blanken et al.*, 2000; *Garratt*, 1992; *Stull*, 1988]

$$H = \rho_a C_P C_H U (T_w - T_a) \tag{17}$$

$$LE = L C_E U (e_w - e_a) \tag{18}$$

where ρ_a is the air density (kg m^{-3}), C_P is specific heat of air (J °C·kg^{-1}), L is latent heat of vaporization, U is the horizontal wind speed (m s^{-1}) at the reference height in the ASL, T_w and T_a are the water surface layer temperature (°C) and the air temperature (°C) at the reference height, e_w and e_a are the vapor pressure (kPa) at the water surface and the reference height, and C_H and C_E are the bulk transfer coefficients for heat and moisture, respectively [*Garratt*, 1992; *Liu et al.*, 2009; *Stull*, 1988].

Previous studies have found good match between estimation using $U(e_w - e_a)$ and the measured LE, as well as between estimation using $U(T_w - T_a)$ and the measured H on a daily basis in the northern lakes [*Blanken et al.*, 2000; *Nordbo et al.*, 2011] or in the cool season in southern lakes [*Liu et al.*, 2009]. In this study it was found that U and $e_w - e_a$ have separate or joint impacts on

LE. Thus it was expected that U and $e_w - e_a$ may play different roles in governing turbulent exchange of LE on different timescales and during different seasons. Our results showed that based on the correlations between half-hourly LE and $U(e_w - e_a)$, the data points were concentrated around the 1:1 line in the cool season (R^2 = 0.79), while widely scattered in the warm season (R^2 = 0.47) (Figure 23). For H, the higher correlations were also present for the cool season (R^2 = 0.84) than the warm season (R^2 = 0.76). Overall, the correlation coefficients were larger for H than LE annually or seasonally (Figure 23). *What processes, then, caused these two distinctive correlation patterns for these two seasons?*

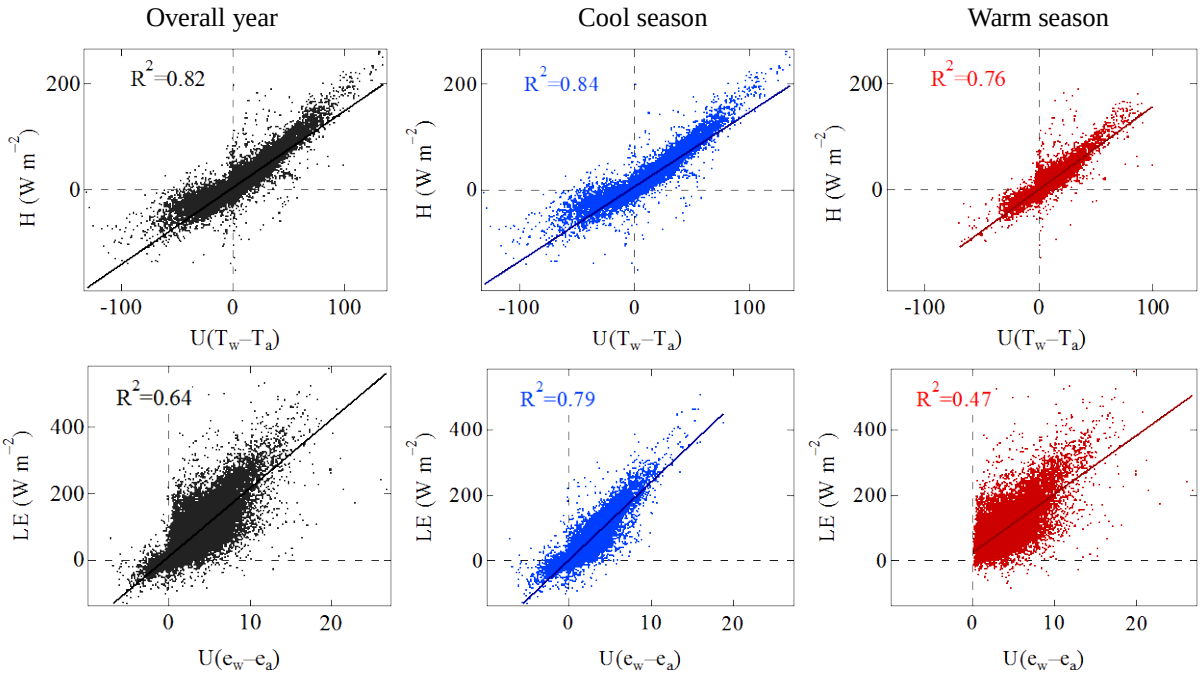

Figure 23. Relationships between half-hourly H and $U(T_w - T_a)$ over the year, in the cool season, and in the warm season (upper panels). Relationships between half-hourly LE and $U(e_w - e_a)$ over the year, in the cool season, and in the warm season (lower panels). All available data points in 2008 and 2009 were used

The nonlinear interaction between U and $e_w - e_a$ on LE requires a detail analysis about their relationships with LE. Therefore, we divided $e_w - e_a$ (hence denoted as Δe) into a number of small, continuous ranges, performed linear regressions of half-hourly LE data against U and Δe in each Δe range, and then discussed the possible causes that led to better relationships between LE and U in some specific Δe ranges. Due to the distinct intraseasonal patterns in the winter (i.e., January, February, and March) and summer (i.e., June, July, and August) (Figure 24), the analyses were conducted separately for these two seasons.

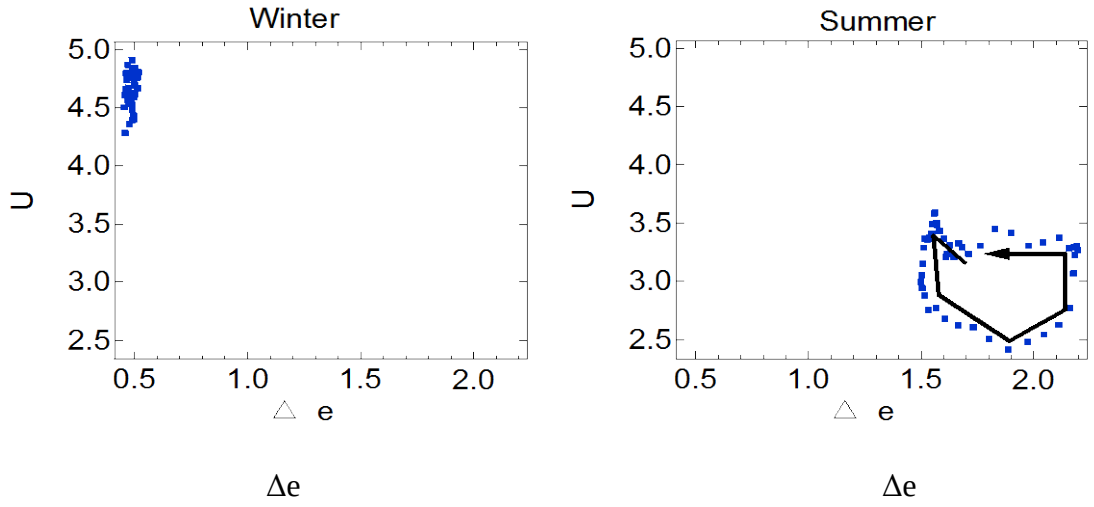

Figure 24. Scatter plots of U against Δe on the diurnal timescale in the winter and summer

In general, our results indicated that LE had poor correlations with Δe in each Δe range in both the winter and summer ($R^2 \leq 0.2$; Figures 25, 26). In contrast, LE was generally in good linear correlation with U in each Δe range, with the slope being larger as Δe increased (Figures 25, 26).

Δe also affected LE but in a different way. When we averaged all LE points to obtain one averaged value for each Δe range and make the same average from U and Δe, and plotted these means against the averaged Δe in Figure 27, we found a very strong correlation between the averaged LE and the averaged Δe ($R^2 = 0.94$).

In winter, Δe was small (0~1.6 kPa) and thus was the limiting factor for LE while U was large (Figure 25). Both U and Δe increased in winter due to the increased numbers of windy days with dry and cold air masses passing over water, leading to stronger linear correlations between LE and UΔe as well as between U and Δe (Figure 27). It is also noted that when Δe was very small (i.e., $\Delta e \leq 0.3$ kPa), LE was also around zero. When Δe became large, the correlation coefficients between LE and U increased. This indicates that when the vapor pressure gradient over water was small, it acts as a limiting factor that even large mechanical mixing (high U, up to 15 m s^{-1}; Figure 25) would not promote LE. When Δe became larger, LE was not limited by Δe and thus was more associated with U than Δe (Figures 25). However, the correlation coefficients between LE and U with the increased Δe approached their maximums when Δe was about 1.0 kPa, and then even decreased when Δe was greater than 1.0 kPa.

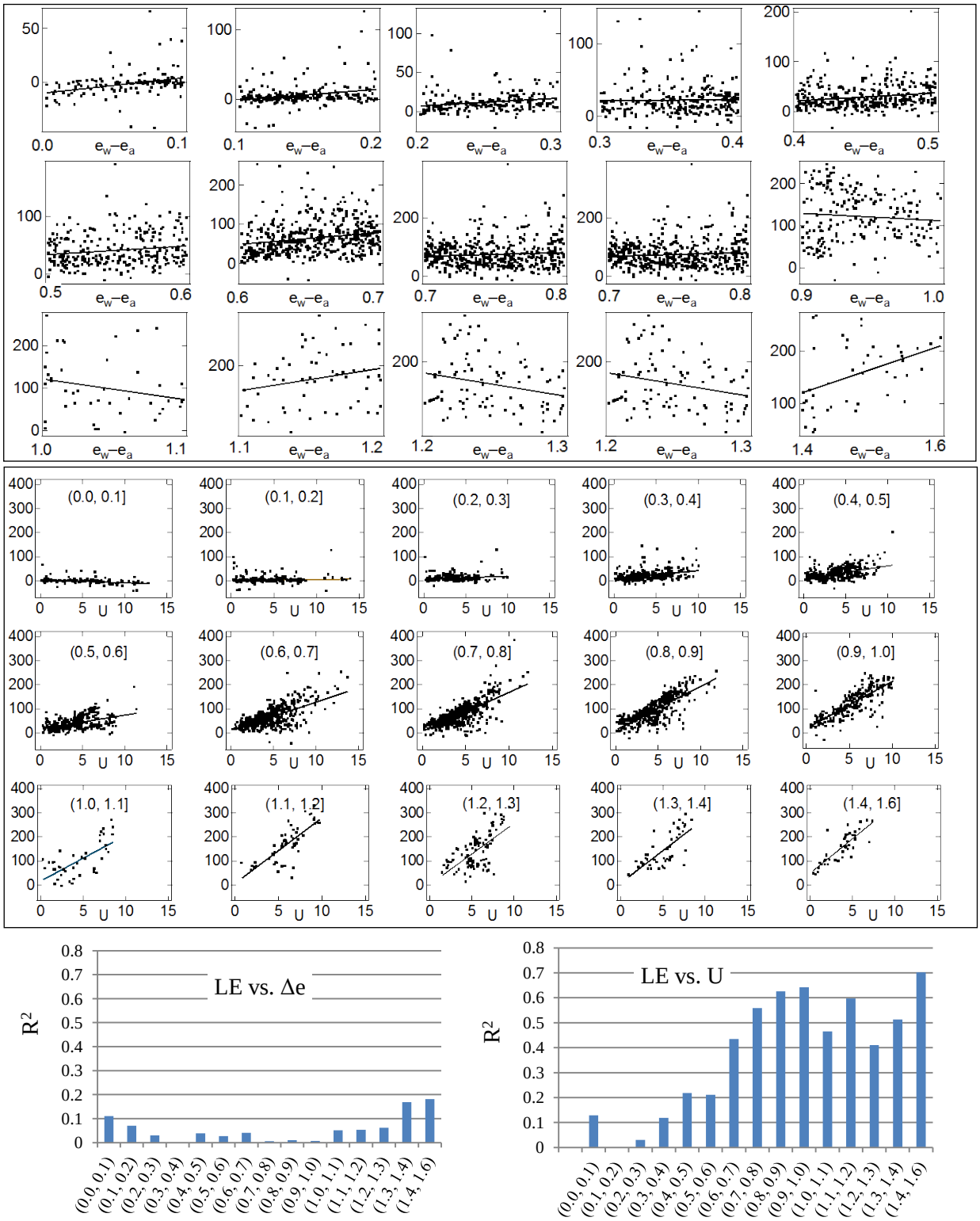

Figure 25. The linear relationship between LE and Δe (upper panels) or U (middle panels) in designated Δe ranges and their correlation coefficients (bottom panels) in winter

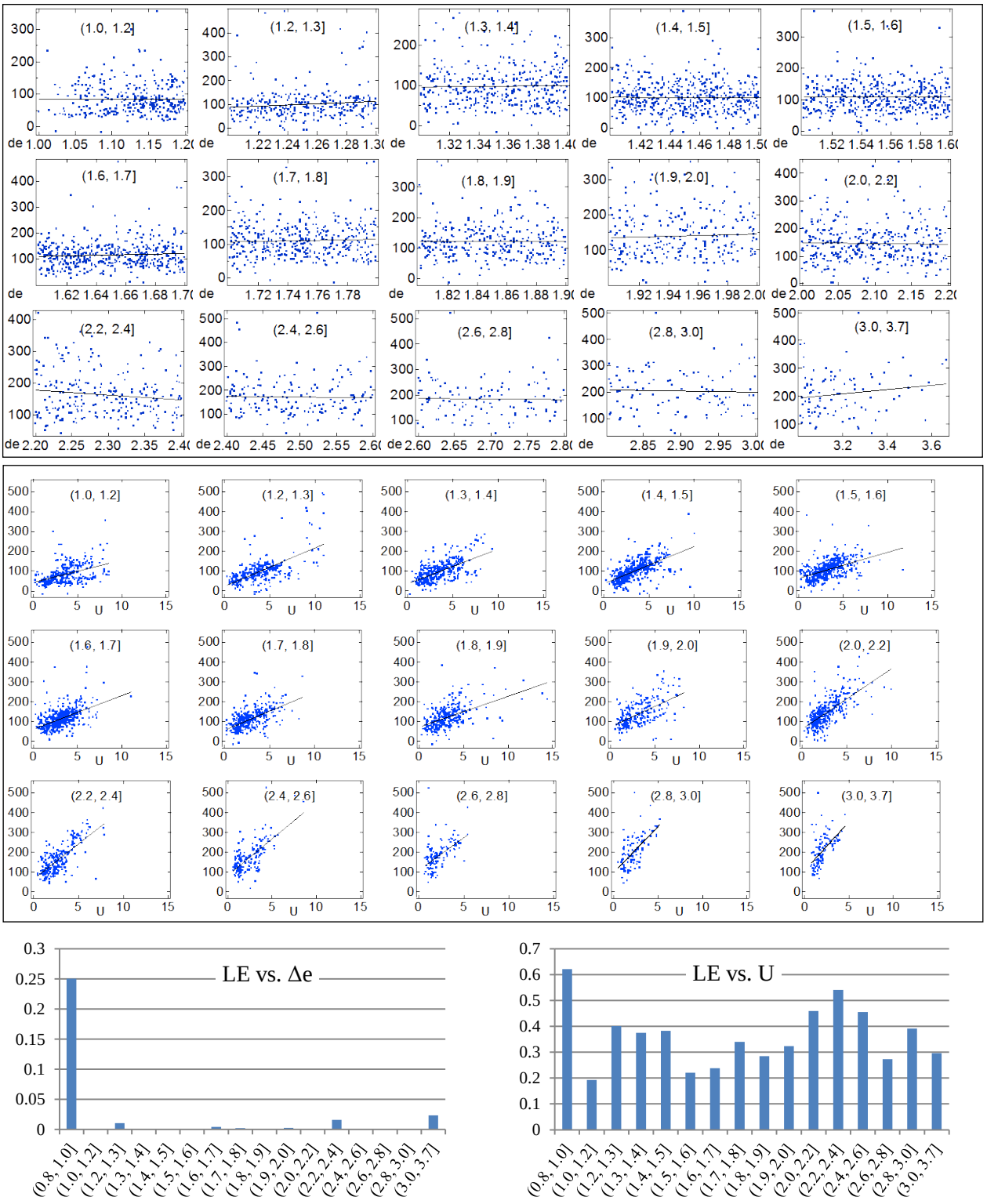

Figure 26. The linear relationships between LE and Δe (upper panels) and between LE and U (middle panels) in designated Δe ranges and their correlation coefficients (bottom panels) in summer

In summer, Δe was relatively large (1 ~ 3.7 kPa) while U were relatively small and acted as a limiting factor for driving LE. Both U and Δe exhibited strong diurnal cycles and sometimes varied at different directions (Figure 26). It is noted that averaged over all Δe ranges, U had a robust negative linear relationship with Δe (R^2 = 0.90; Figure 27). When U and Δe did not change at the same direction during a day; the variations in LE were not well quantified by UΔe, leading to the weakened correlation relationship between LE and UΔe (Figures 27)

In summary, LE was under the joint influences of Δe and U, with Δe determining its magnitude and U determining its variations.

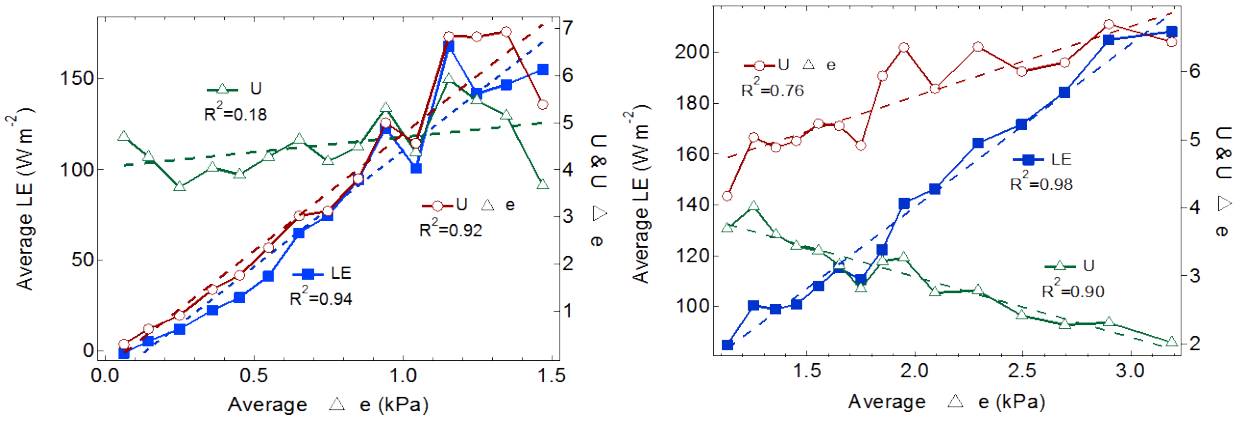

Figure 27. Relationships of LE, U, and Δe for different Δe ranges in winter and summer. All values are averaged in the same Δe range. It shows that LE is strongly related with Δe between ranges. Also, U is positively correlated with Δe in the winter, and negatively correlated with Δe in the summer

3.8 Comparison of the surface energy budget with high-latitude northern lakes

In this section, the annual and seasonal surface energy budget over a large low-latitude water body, the Ross Barnett Reservoir (hereafter RBR, in this study) and over a typical large high-latitude lake, the Great Slave Lake (hereafter GSL), were compared and analyzed. We adopted the eddy covariance data over GSL which were measured in 1999 and reported by *Blanken* et al. [2000] and *Rouse* et al. [2003]. RBR was ice-free throughout the year, while GSL was ice-free for 192 days on average in a year, and covered with ice for an average of 173 days (Table 10). The GSL ice-free season was typically between June 1–15 and December 15 to January 1 [*Rawson*, 1950]. H and LE were only available for the ice-free season. In addition, the area and mean depth for GSL were much larger than RBR (Table 10), leading to larger water heat storage capacity for GSL.

3.8.1 Comparison of the annual mean surface energy budget and cumulative evaporation

Previous studies have focused on the evaporation regime over high-latitude lakes [*Blanken et al.*, 2003; *Blanken et al.*, 2008; *Blanken et al.*, 2000; *Rouse et al.*, 2003; *Rouse et al.*, 2008; *Rouse et al.*, 2005; *Schertzer et al.*, 2003]. The annual mean LE and cumulative evaporation (hereafter cumE) in GSL and RBR are listed in Table 10. Note that the annual mean LE (unit: W m^{-2}) and cumE (unit: mm) were linked through Eq. (19)

$$cumE = \frac{LE}{L \times 10^3} \times Days \times 24 \times 60 \times 60 \quad (19)$$

where L is the latent heat of vaporization for water, Days are the ice-free periods for the lakes.

On an annual basis, it is evident that RBR has much larger LE and cumE (i.e., annual mean LE = 83 W m^{-2}, cumE = 1156 mm) than GSL (i.e., annual mean LE = 59 W m^{-2}, cumE = 432 mm) (Table 10). This indicates that both LE and evaporation have larger magnitudes for RBR than in GSL, suggesting that evaporative water loss from low-latitude lakes are likely to be more significant compared with those in high-latitude lakes. In addition, Rn was smaller in GSL (i.e., Rn in 2009 <101 W m^{-2}) than in RBR (i.e., annual mean Rn = 108 W m^{-2}), indicating less energy input to the water surface. H was likely to be larger in GSL (i.e., >22 W m^{-2}) than in RBR (i.e., annual mean H = 16 W m^{-2}) (Table 10), indicating more heat was transferred into the atmosphere through H in high-latitude lakes than in RBR.

Interannual variations were also evident for both water bodies. However, in RBR which is ice free, interannual variations in H and LE are mainly caused by interannual variations in H and LE pulses (e.g., their durations, intensity, and frequency) as well as Rn. On the contrary, the final ice breakup date is found to be the most important factor affecting the interannual variations in the surface energy balance over GSL [*Rouse et al.*, 2005]. Earlier ice breakups lead to more energy absorption of solar radiation which reaches its maximum in June, earlier heating of the lake, and

hence sooner the changes from stable to unstable over-lake ASL regimes. In addition, earlier breakups are highly likely related to longer ice-free periods, resulting in larger cumE in GSL (Table 10).

Table 10. Comparison of the annual mean LE and annual cumulative evaporation (cumE) over a low-latitude water body (in this study) and a high-latitude lake (GSL). All studies used direct measurements from eddy covariance systems. Both LE and cumE were apparently larger over RBR than over GSL. Ref – reference sources for studies: 1) Blanken et al. [2000]; 2) Rouse et al. [2003]; 3) Oswald and Rouse [2004]; 4) the present study.

Location	Area km^2	Mean Depth m	Ice-free Period	Days	Rn W m^{-2}	H W m^{-2}	LE W m^{-2}	cumE mm	Ref
			Great Slave Lake (GSL)						
61.92°N,	28568	32	20 Jun–13 Dec 1997	176			57	386	1
113.73°W			1 Jun 1998–8 Jan 1999	221			57	485	1
			12 Jun–13 Dec 1999	184	<101	>22	59	417	2
			6 Jun–9 Dec 2000	186			62	439	3
Mean				**192**			**59**	**432**	
			Ross Barnett Reservoir (RBR)						
32.44°N,	134	5	Annual 2008	365	109	17	87	1211	4
90.03°W			Annual 2009	365	106	15	79	1101	4
Mean				**365**	**108**	**16**	**83**	**1156**	

3.8.2 Comparison of seasonal variations in the surface energy budget

Seasonal variations in the surface energy budget were significantly different between GSL and RBR. At the beginning and the end of the year, solar radiation was close to zero over GSL while it was approximately 100 W m^{-2} over RBR, indicating less energy input to the water surface for high-latitude lakes in the winter (Figure 28). As the months progressed, solar radiation shared

similar bell-shapes over both water bodies. Rn over GSL was negative during the roughly first four months and lasted two months of the year, while Rn over RBR remained positive across the year. Interestingly, Rn did not increase to exceed zero until May in GSL, while it generally followed solar radiation over RBR (Figure 28). This lag in increasing and in achieving positive Rn was controlled by the extent of ice melt over the lake [*Rouse et al.*, 2005].

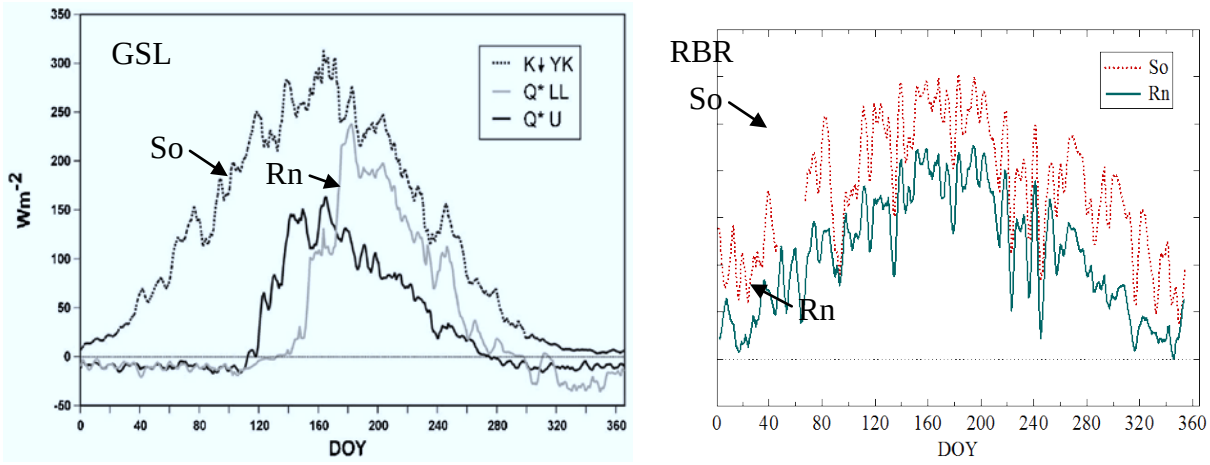

Figure 28. Comparison of annual radiation cycles between a large high-latitude lake (left, GSL) and a large low-latitude water body (right, RBR). The 5-day running means were presented. The left GSL plot was adopted from Rouse et al. [2005].

Seasonal variations in LE, H, and z/L over GSL exhibited significantly different patterns from those of RBR (Figure 29). In general, LE and H over GSL were similar and smallest at the beginning of the ice-free season, increased gradually as the months progressed into winter, and reached maximum before the water was covered with ice. Since Rn decreased after its maximum in June and July, which corresponded to the beginning of the ice-free season, both LE and H were apparently disconnected with Rn. In fact, the seasonal variations in LE and H over GSL

were found to be best explained by the seasonal variations in z/L over the water surface [*Blanken et al.*, 2000; *Rouse et al.*, 2003]. According to z/L, the ice-free season can be divided into two stages: the heating stage and the cooling stage. The heating stage lasted from the final ice breakup in June till mid- to late August, during which T_w was smaller than T_a, leading to a negative temperature gradient and a stable atmosphere (reflected by positive z/L) over the water (Figure 29). LE and H were suppressed during this stage and Rn was mainly used to heat the water.

The cooling stage started thereafter till its freeze up, during which T_w exceeded T_a, creating a positive temperature gradient and an unstable atmosphere (reflected by negative z/L, Figure 29), and leading to largely promoted LE and H. During the cooling stage, Rn was small and LE and H were large, indicating the energy previously stored in the water in the heating stage was released into the atmosphere in the form of LE and H. Note that the magnitude of LE during the cooling stage of GSL was close to that in the warm season of RBR. H was much larger during the cooling stage of GSL than in the cool season of RBR. The absolute magnitudes of z/L over GSL generally had larger magnitudes, whether positive or negative, than those over RBR. However, z/L was typically negative over RBR throughout the year, indicating typical unstable over-water ASL conditions over low-latitude water bodies.

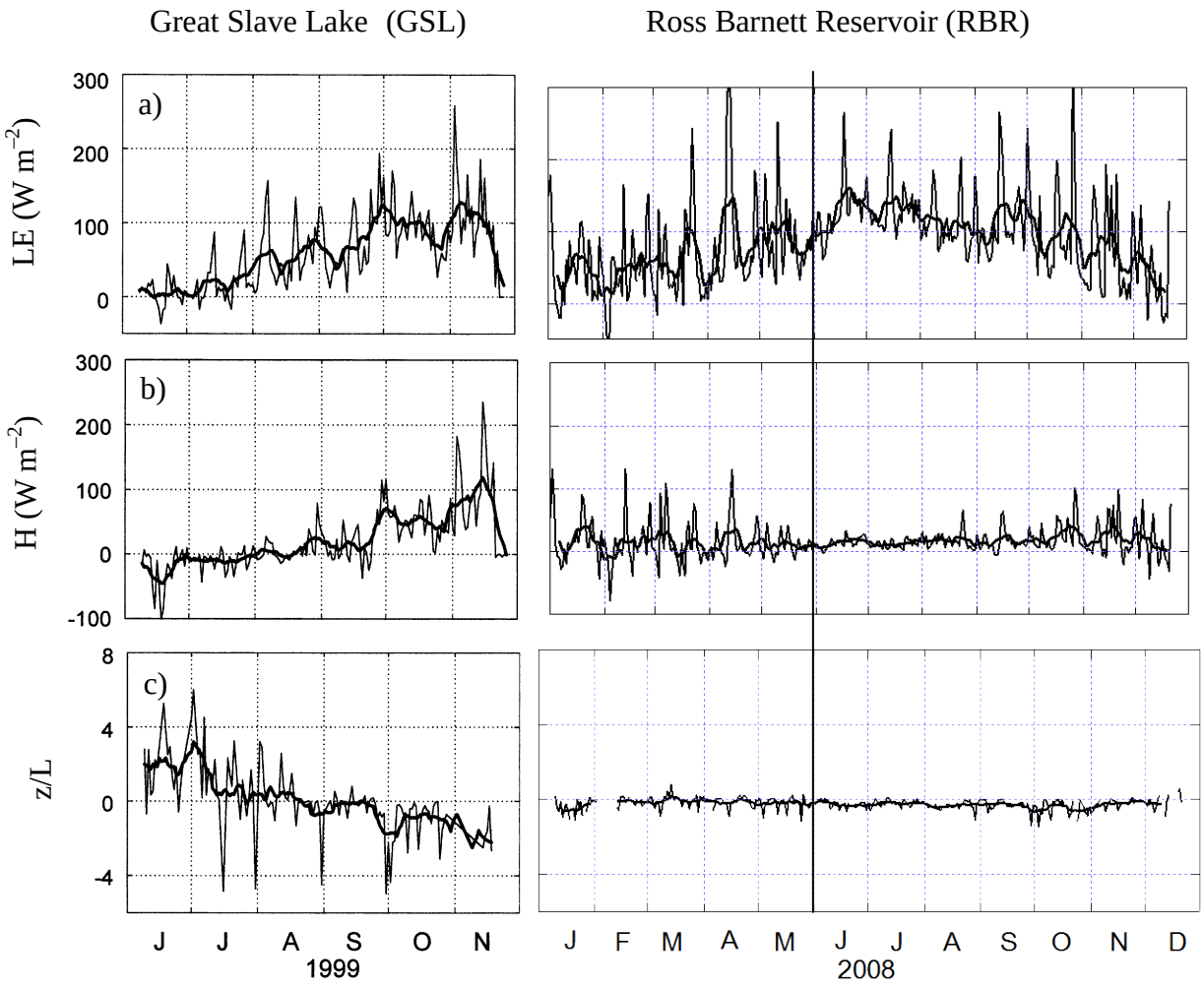

Figure 29. Comparison of the annual patterns of a) the latent heat flux (LE), b) the sensible heat flux (H), and c) the atmospheric surface layer stability (z/L) between a low-latitude lake (present study) and a high-latitude lake (the Great Slave Lake). The patterns of the daily means (thin lines) are illustrated by 10-day running means (thick lines). Plots for the Great Slave Lake were adopted from Blanken et al. [2000].

Large LE and H pulses were also evident for GSL during the ice-free period. Previous studies found these pulses were due to strong wind activities which enhanced turbulent exchanges. This shows that the surface energy budget over the high-latitude lakes was also influenced by high-wind events, similar with this low-latitude water body as discussed earlier in this study.

4. Summary and conclusions

In this study, we have analyzed the seasonal, diurnal, and interannual variations in the surface energy budget using eddy covariance and meteorological measurements in 2008 and 2009 over a large southern inland water body. The factors controlling H and LE as well as H and LE pulses were also identified on these timescales. We obtained the following conclusions.

1. The annual means of Rn, H, and LE for the two years were 110.6, 15.7, and 83.7 W m^{-2}, respectively. About 81% of Rn absorbed by water was transferred to the atmosphere through LE and the remainder was transferred by H. Throughout the year, the unstable stratified ASL, as well as positive temperature and humidity gradients were observed on a half-monthly average basis, although negative gradients occurred during certain short periods of time when the over-water air masses were warmer and wetter than the water surface. $T_w - T_a$ was the primary factor affecting seasonal variation patterns in H, and including U improved this relation. Seasonal variations in LE were best explained by similar variations in $e_w - e_a$ followed by Rn.

2. On the diurnal timescale, the ASL was unstable (particularly, the ASL was strongly unstable in the early morning) except for a short period in the late afternoon in which the ASL was weakly stable. H displayed clear diurnal cycles with maximums in the early morning and minimums in the late afternoon. Two diurnal variation patterns were present for LE (1) LE followed the

diurnal variation pattern of H for the cool season (this pattern was relatively weak) and (2) LE displayed a bell-shape with maximums in the late afternoon in the warm season. Different meteorological variables played different roles in controlling diurnal variations in H and LE. H generally followed the diurnal cycle of $T_w - T_a$ throughout the year, which resulted mainly from the large daily variations in T_a. The diurnal cycle of LE was strongly influenced by ASL stability in the winter, and was alternately affected by U and $e_w - e_a$ in the summer, leading to a phase lag typically between LE and $U(e_w - e_a)$. Both H and LE showed no correspondence in their diurnal cycles to those of Rn, reflecting that Rn was not the direct driving force for H and LE on a diurnal timescale.

3. Intraseasonal and seasonal variations in turbulent exchanges of H and LE were strongly modulated by H and LE pulses that were associated with dry, cold air masses brought by northerly winds during high-wind events (i.e., cold fronts). During these pulses, both thermally and mechanically generated turbulent fluxes were greatly enhanced, in correspondence to the large temperature and vapor pressure gradients, and high wind speed, respectively, at the water-air interface. More pulses occurred in the cool season than in the warm season. These pulses contributed 68% and 48% to the overall H and LE in the cool season, respectively, and 30% and 17% in the warm season, respectively. The contribution of pulses to the overall H and LE fluxes were consistent during the two years, contributing approximately 50% of the overall H

and 28% of the overall LE.

4. H and LE were mainly controlled by different meteorological factors on different timescales and in different seasons. For the entire year, H was best explained by $U(T_w - T_a)$ on a daily basis ($R^2 = 0.92$), while LE by $U(e_w - e_a)$ on the half-monthly basis ($R^2 = 0.86$). LE had consistently better linear relationships between $U(e_w - e_a)$ and H in the cool season, due to the promotion of both H and LE during H and LE pulse days, as compared with the warm season. U was found to play an important role in affecting LE on the 30-min timescale. When $e_w - e_a$ was small and acted as a limiting factor, LE was mainly determined by the available $e_w - e_a$. When $e_w - e_a$ was not a limiting factor, LE generally closely followed the variations in U. Since $e_w - e_a$ and U did not always change in the same direction, the phase lags were generated when explaining the relationship between the measured LE and $U(e_w - e_a)$.

5. The interannual variations in the surface energy budget between 2008 and 2009 was mainly caused by their variations during the cool season, when 2008 was provided with more available energy (Rn) during the non-pulse days and experienced stronger high-wind events during the pulse days. This was consistent with the larger Rn and U in 2008. It was shown that pulses significantly contributed to the interannual variations in H and LE fluxes. About 80% and 20% of interannual variations in H were attributed to those in pulses and non-pulse days, respectively,

while about 40% and 60% of interannual variations in LE were coming from those in pulses and non-pulse days, respectively. In addition, it was speculated that in this region southerly winds with warm and humid air masses generally suppressed H and LE, while strong northerly winds with cool and dry air masses caused H and LE pulse events and promoted H and LE. Therefore, interannual variations in wind direction and wind speed are likely to contribute partly to those in H and LE fluxes in this region, as more northerly winds with higher wind speed resulted in larger H and LE in 2008 than in 2009. Our results suggest that possible shifts in northerly and southerly winds associated with changes in synoptic weather activities, which affect the H and LE pulse events in terms of frequency, duration, and intensity, would have significant impacts on seasonal, annual, and interannual variations in the water surface energy budget, evaporation rates, and hydrologic processes of this region.

6. The comparison of the surface energy budget between lakes from low- and high-latitudes showed that larger LE and smaller H occurred in low-latitude lakes than in high-latitude lakes. This indicates that water vapor loss were more significant for low-latitude lakes while sensible heat transfer were more important for high-latitude lakes. Interannual variations in the surface energy budget of high-latitude lakes were most strongly associated with the final ice breakup date, which were likely to result in longer ice-free periods. Seasonal variations in H and LE were significantly different for low- and high-latitude lakes. In contrast to the significant contribution

of H and LE pulses to the surface energy budget of low-latitude lake studied in this region, H and LE in high-latitude lakes were generally best explained by the over-water atmospheric stability. A heating stage and a cooling stage were distinguished according to the positive and negative signs of z/L, respectively. During the heating stage, H and LE were suppressed and Rn was mostly used for heating the water. During the cooling stage, H and LE were promoted and Rn was small, leading to releases of previously stored energy of the water into the atmosphere. High-wind events were found to have significant effects to lakes in both latitudes.

7. This study has shown that this low-latitude water body has distinct seasonal and interannual variations in the surface energy budget as a result of the joint effects of over-water meteorological variables and synoptic weather conditions. This study reported various aspects of the surface energy budget for two years, filled the gaps of long-term direct flux measurements over low-latitude inland waters, and provided analyses in physical processes controlling H and LE. These results will assist in validating and developing better regional weather/climate models, as well as in local water resource management in terms of evaporative water loss from low-latitude inland waters.

References

Ahrens, C. D. (2011), *Essentials of meteorology :an invitation to the atmosphere*, 6th ed., xvii, 506 pp., Brooks/Cole, Belmont, CA.

Bates, G. T., S. W. Hostetler, and F. Giorgi (1995), Two-year simulation of the great-lakes region with a coupled modeling system, *Mon. Weather Rev.*, *123*(5), 1505-1522.

Blanken, P. D., W. R. Rouse, and W. M. Schertzer (2003), Enhancement of evaporation from a large northern lake by the entrainment of warm, dry air, *Journal of Hydrometeorology*, *4*(4), 680-693.

Blanken, P. D., W. Rouse, and W. Schertzer (2008), The time scales of evaporation from Great Slave Lake, in *Cold Region Atmospheric and Hydrologic Studies. The Mackenzie GEWEX Experience, Volume 2: Hydrologic Processes*, edited, pp. 181-196, Springer, Berlin.

Blanken, P. D., W. R. Rouse, A. D. Culf, C. Spence, L. D. Boudreau, J. N. Jasper, B. Kochtubajda, W. M. Schertzer, P. Marsh, and D. Verseghy (2000), Eddy covariance measurements of evaporation from Great Slave Lake, Northwest Territories, Canada, *Water Resources Research*, *36*(4), 1069-1077.

Bonan, G. B. (1995), Sensitivity of a GCM simulation to inclusion of inland water surfaces, *Journal of Climate*, *8*(11), 2691-2704.

Budyko, M. I. (1974), *Climate and life*, xvii, 508 pp., Academic Press, New York.

Cole, J. J., et al. (2007), Plumbing the global carbon cycle: integrating inland waters into the terrestrial carbon budget, *Ecosystems*, *10*(1), 172-185.

Eaton, A. K., W. R. Rouse, P. M. Lafleur, P. Marsh, and P. D. Blanken (2001), Surface energy balance of the western and central Canadian subarctic: Variations in the energy balance among five major terrain types, *Journal of Climate*, *14*(17), 3692-3703.

Finnigan, J. J., R. Clement, Y. Malhi, R. Leuning, and H. A. Cleugh (2003), A re-evaluation of long-term flux measurement techniques - Part I: Averaging and coordinate rotation, *Boundary-Layer Meteorology*, *107*(1), 1-48.

Foken, T. (2008), *Micrometeorology*, 1st ed., Springer, New York.

Foken, T., R. Leuning, S. Oncley, M. Mauder, and M. Aubinet (2012), Corrections and data

quality, in *Eddy Covariance: A Practical Guide to Measurement and Data Analysis*, edited by M. Aubinet, Vesala, T., Papale, D., Springer, Dordrecht, Heidelberg, London, New York.

Garratt, J. R. (1992), *The atmospheric boundary layer*, xviii, 316 pp., Cambridge University Press, Cambridge, New York.

Hendersonsellers, B. (1986), Calculating the surface-energy balance for lake and reservoir modeling: A review, *Rev. Geophys.*, *24*(3), 625-649.

Hojstrup, J. (1993), A statistical-data screening-procedure, *Meas. Sci. Technol.*, *4*(2), 153-157.

Hostetler, S. W., and P. J. Bartlein (1990), Simulation of lake evaporation with application to modeling lake level variations of Harney-Malheur Lake, Oregon, *Water Resources Research*, *26*(10), 2603-2612.

Huntington, T. G. (2006), Evidence for intensification of the global water cycle: Review and synthesis, *Journal of Hydrology*, *319*(1-4), 83-95.

Lenters, J. D., T. K. Kratz, and C. J. Bowser (2005), Effects of climate variability on lake evaporation: Results from a long-term energy budget study of Sparkling Lake, northern Wisconsin (USA), *Journal of Hydrology*, *308*(1-4), 168-195.

Liu, H., G. Peters, and T. Foken (2001), New equations for sonic temperature variance and buoyancy heat flux with an omnidirectional sonic anemometer, *Boundary-Layer Meteorology*, *100*(3), 459-468.

Liu, H., J. T. Randerson, J. Lindfors, and F. S. Chapin (2005), Changes in the surface energy budget after fire in boreal ecosystems of interior Alaska: An annual perspective, *J. Geophys. Res.-Atmos.*, *110*(D13).

Liu, H., P. D. Blanken, T. Weidinger, A. Nordbo, and T. Vesala (2011), Variability in cold front activities modulating cool-season evaporation from a southern inland water in the USA, *Environmental Research Letters*, *6*(2), 024022.

Liu, H., Y. Zhang, S. Liu, H. Jiang, L. Sheng, and Q. L. Williams (2009), Eddy covariance measurements of surface energy budget and evaporation in a cool season over southern open water in Mississippi, *Journal of Geophysical Research*, *114*(D4).

Lofgren, B. M. (1997), Simulated effects of idealized Laurentian Great Lakes on regional and large-scale climate, *Journal of Climate*, *10*(11), 2847-2858.

Long, Z., W. Perrie, J. Gyakum, D. Caya, and R. Laprise (2007), Northern lake impacts on local seasonal climate, *Journal of Hydrometeorology*, *8*(4), 881-896.

MacIntyre, S., J. O. Sickman, S. A. Goldthwait, and G. W. Kling (2006), Physical pathways of nutrient supply in a small, ultraoligotrophic arctic lake during summer stratification, *Limnol. Oceanogr.*, *51*(2), 1107-1124.

Magnuson, J. J., et al. (2000), Historical trends in lake and river ice cover in the Northern Hemisphere, *Science*, *289*(5485), 1743-1746.

Mauder, M., and T. Foken (2004), Documentation and instruction manual of the eddy covariance software Package, *http://www.geo.unibayreuth.de/mikrometeorologie/ARBERG/ARBERG26.pdf*.

Mauder, M., O. O. Jegede, E. C. Okogbue, F. Wimmer, and T. Foken (2006), Surface energy balance measurements at a tropical site in West Africa during the transition from dry to wet season, *Theoretical and Applied Climatology*, *89*(3-4), 171-183.

McCabe, G. J., M. P. Clark, and M. C. Serreze (2001), Trends in Northern Hemisphere surface cyclone frequency and intensity, *Journal of Climate*, *14*(12), 2763-2768.

Nordbo, A., S. Launiainen, I. Mammarella, M. Leppäranta, J. Huotari, A. Ojala, and T. Vesala (2011), Long-term energy flux measurements and energy balance over a small boreal lake using eddy covariance technique, *Journal of Geophysical Research*, *116*(D2).

Oswald, C. J., and W. R. Rouse (2004), Thermal characteristics and energy balance of various-size Canadian Shield lakes in the Mackenzie River basin, *Journal of Hydrometeorology*, *5*(1), 129-144.

Rawson, D. S. (1950), The physical limnology of Great Slave Lake, *J. Fish. Res. Board Can.*, *8*, 3-66.

Rouse, W. R., C. M. Oswald, J. Binyamin, P. D. Blanken, W. M. Schertzer, and C. Spence (2003), Interannual and seasonal variability of the surface energy balance and temperature of central Great Slave Lake, *Journal of Hydrometeorology*, *4*(4), 720-730.

Rouse, W. R., P. D. Blanken, N. Bussières, A. E. Walker, C. J. Oswald, W. M. Schertzer, and C. Spence (2008), An investigation of the thermal and energy balance regimes of Great Slave and Great Bear Lakes, *Journal of Hydrometeorology*, *9*(6), 1318-1333.

Rouse, W. R., C. J. Oswald, J. Binyamin, C. R. Spence, W. M. Schertzer, P. D. Blanken, N.

Bussieres, and C. R. Duguay (2005), The role of northern lakes in a regional energy balance, *Journal of Hydrometeorology*, *6*(3), 291-305.

Sacks, L. A., T. M. Lee, and M. J. Radell (1994), Comparison of energy-budget evaporation losses from two morphometrically different Florida seepage lakes, *Journal of Hydrology*, *156*(1-4), 311-334.

Sakai, R. K., D. R. Fitzjarrald, and K. E. Moore (2001), Importance of low-frequency contributions to eddy fluxes observed over rough surfaces, *J. Appl. Meteorol.*, *40*(12), 2178-2192.

Schertzer, W. M., W. R. Rouse, P. D. Blanken, and A. E. Walker (2003), Over-lake meteorology and estimated bulk heat exchange of Great Slave Lake in 1998 and 1999, *Journal of Hydrometeorology*, *4*(4), 649-659.

Schotanus, P., F. T. M. Nieuwstadt, and H. A. R. Debruin (1983), Temperature-measurement with a sonic anemometer and its application to heat and moisture fluxes, *Boundary-Layer Meteorology*, *26*(1), 81-93.

Solomon, S., Intergovernmental Panel on Climate Change., and Intergovernmental Panel on Climate Change. Working Group I. (2007), *Climate change 2007: the physical science basis :contribution of Working Group I to the Fourth Assessment Report of the Intergovernmental Panel on Climate Change*, viii, 996 pp., Cambridge University Press, Cambridge ; New York.

Stannard, D. I., and D. O. Rosenberry (1991), A comparison of short-term measurements of lake evaporation using eddy-correlation and energy budget methods, *Journal of Hydrology*, *122*(1-4), 15-22.

Stull, R. B. (1988), *An introduction to boundary layer meteorology*, xii, 666 pp., Kluwer Academic Publishers, Dordrecht ; Boston.

Sturrock, A. M., T. C. Winter, and D. O. Rosenberry (1992), Energy budget evaporation from Williams Lake - a closed lake in north central Minnesota, *Water Resources Research*, *28*(6), 1605-1617.

Teng, H., W. Washington, and G. Meehl (2008), Interannual variations and future change of wintertime extratropical cyclone activity over North America in CCSM3, *Climate Dynamics*, *30*(7), 673-686.

Vallet-Coulomb, C., D. Legesse, F. Gasse, Y. Travi, and T. Chernet (2001), Lake evaporation

estimates in tropical Africa (Lake Ziway, Ethiopia), *245*(1–4), 18.

Vesala, T., J. Huotari, Ü. Rannik, T. Suni, S. Smolander, A. Sogachev, S. Launiainen, and A. Ojala (2006), Eddy covariance measurements of carbon exchange and latent and sensible heat fluxes over a boreal lake for a full open-water period, *Journal of Geophysical Research*, *111*(D11).

Vickers, D., and L. Mahrt (1997), Quality control and flux sampling problems for tower and aircraft data, *J. Atmos. Oceanic Technol.*, *14*(3), 512-526.

Walter, K. M., S. A. Zimov, J. P. Chanton, D. Verbyla, and F. S. Chapin (2006), Methane bubbling from Siberian thaw lakes as a positive feedback to climate warming, *Nature*, *443*(7107), 71-75.

Webb, E. K., G. I. Pearman, and R. Leuning (1980), Correction of flux measurements for density effects due to heat and water-vapor transfer, *Q. J. R. Meteorol. Soc.*, *106*(447), 85-100.

Winter, T. C., D. C. Buso, D. O. Rosenberry, G. E. Likens, A. M. Sturrock, and D. P. Mau (2003), Evaporation determined by the energy-budget method for Mirror Lake, New Hampshire, *Limnol. Oceanogr.*, *48*(3), 995-1009.